4.10 The Effect of Waste Tires on LFG Emissions

4.10.1 LFG Production from Waste Tires

In 2017, the USEPA estimated that 6.5 million tons of waste tires (~290 million tires, cars, trucks, motorcycles) were generated in the US, constituting, 2.4%, of the total MSW generated (USEPA 2017c). In California, CalRecycle estimates that approximately 51.1 million waste tires were generated in 2018 alone, which is 18% of the nationwide total (CalRecycle 2018b). At end of life, three primary pathways for waste tire processing are currently in use: recycling, combustion with energy recovery, and landfilling (USEPA 2017c). USEPA has estimated that, approximately, 40, 40 and 20% of waste tires are recycled, combusted, and landfilled on an annual basis (USEPA 2017c). Due to their size, shape, and physiochemical composition, waste tires typically do not readily degrade in the environment (Conesa et al. 2004, Stevenson et al. 2008). In general, natural (bio) degradation of rubber materials in tires is a slow process (Romine and Romine 1997, Holst et al. 1998). High concentrations of toxic chemicals, such as poly-cyclic aromatic hydrocarbons, phthalates, antioxidants (i.e., zinc oxides), and benzothiazoles have been identified in tires (Menichinni et al. 2011, Llompart et al. 2013). Disposal of waste tires in the landfill environment have high risks, as landfill temperatures, oxygen levels, and leachate are elevated, depleted, and highly acidic, potentially promoting the physical, chemical, and biological transformation or physical and chemical partitioning of these chemicals into more mobile aqueous or gaseous phases (Aydilek et al. 2006, Reddy et al. 2010). The environmental factors governing the decomposition of waste tire materials is complex and primarily depends on the composition of the materials, which vary widely across different manufacturers and automotive classification (car truck, motorcycle) (Aprem et al. 2003). Waste tires consist of vulcanized rubber with steel or fabric belts and reinforcing textile cords (Edil 2008). The tire rubber is a blend of natural and synthetic rubbers. Natural rubber is a biopolymer consisting of repeating poly(cis-1,4-isoprene) units. To improve the durability and elasticity of natural rubber for tire applications, a process termed vulcanization is used. Vulcanization of natural rubber involves covalently bonding the polyisoprene chains with mono, di-, and polysulfide bridges, where the properties of a given rubber material depend on the type and quantity of cross links formed (Aprem et al. 2003). The most commonly used tire rubber (SBR) is a synthetic tire rubber obtained from radiation-based vulcanization of natural rubber latex in the presence of styrene (~25%) and butadiene (~75%) (Dodds et al. 1983, Chaudhari et al. 2005). The radiative based synthetic tires have lower amount of residual toxic chemicals such as zinc oxides or nitrosamines, which improve the biodegradability of the materials (Chaudhari et al. 2005). Waste tire materials also contain carbon black, extender oil, as well as other accelerators such as zinc oxide, stearic acid, and elemental sulfur.

Of the many processes affecting the stability of waste tire composition in the landfill environment, anaerobic/aerobic biological degradation is potentially the most significant transformation pathway. Biodegradation of waste tires consists of three interconnected steps including detoxification, desulfurization, and degradation, all of which are carried out by different microorganisms under varying environmental conditions (summarized in Stevenson et al. 2008). The first step of waste tire

biodegradation, detoxification, involves the removal of chemical compounds that inhibit microbial growth including zinc oxide, salts, aromatic hydrocarbons, and other xenobiotic compounds. Waste tire detoxification is mediated by select species of fungi and bacteria. White rot fungi are xenobiotic degraders that likely metabolize aromatic compounds present in the waste tires under both aerobic and anaerobic conditions (Bredberg et al. 2002). In addition, some bacteria, such as *Rhodococcous rhodochrous*, degrade 2-mercaptobenzothiazole (MBT), a compound commonly used as a vulcanization accelerator (Haroune et al. 2004). Other bacterial genera such as *Corynebacteria*, *Pseudomonas*, and *Escherichia coli* detoxify MBT and other toxic inhibitors (Haroune et al. 2004).

Following detoxification, the elemental sulfur present in the tire waste material is then open to attack by different sulfur oxidizing or reducing bacterial species in a process termed desulfurization (Stevenson et al. 2008). In this stage, the sulfur cross links present in the vulcanized rubber are removed by aerobic oxidizing or anaerobic reducing activity of different sulfur utilizing bacteria (Christiansson et al. 1998). Desulfurization exposes the underlying isoprene polymers that are then available for degradation by other groups of bacteria. In the landfill environment, it is likely that anaerobic conditions persist throughout much of the waste mass, favoring the anaerobic reduction of elemental sulfur to different reduced sulfur compounds (RSC) such as hydrogen sulfide, carbonyl sulfide, carbon disulfide, dimethyl sulfide, and dimethyl disulfide. The reduced forms of elemental sulfur are generally highly volatile and present in the gaseous form, leading to a detectable presence in LFG (Kim 2006).

Polyisoprene polymers composing the initial structure of natural rubber are further broken down during the stage of ultimate degradation of rubber (Rose and Steinbuchel 2005, Stevenson et al. 2008). Two main groups of rubber metabolizing organisms have been identified, including clear zone forming bacteria and adhesively growing bacteria. Clear zone forming bacteria include members of the genera *Streptomyces*, *Xanthomonas*, *Micromonospora*, *Thermomonospora*, and *Actinomyces*, which use latex as a sole carbon and energy source (Rose and Steinbuchel 2005). The other group of bacteria form biofilms (adhesive growth) on the rubber material in order to metabolize rubber and include bacteria from the genera: *Gordonia*, *Corynebacterium*, *Mycobacterium*, *Pseudomonas,* and *Nocardia* (Rose and Steinbuchel 2005, Roy et al. 2006). The intermediate and end products of this metabolism vary from ketones, to aldehydes, to organic acids (i.e., carboxylic acids) (Rose et al. 2005). Considering all of these interconnected stages of biodegradation, the overall rate of anaerobic waste tire decomposition depends on many factors, including the presence of microorganisms specific to each stage and favorable environmental conditions (i.e., moisture, temperature, pH, nutrients, oxygen level) to support the growth of these microorganisms within the landfill environment. It is likely that the level of processing of waste tires prior to landfill disposal (i.e., whole tires, chips, aggregates) highly influences the susceptibly and rate of biological degradation of waste tire materials, where finer materials may improve biodegradation rates. As tires adsorb different toxic chemicals and the organisms that degrade these compounds are rare and potentially

site-specific, detoxification may be the rate limiting step of this multi-stage process (Baykal et al. 1992, Park et al. 1996, Edil et al. 2004).

4.10.2 Potential Impacts on Emissions

The presence of waste tires has potential effects on the physical and mechanical stability of the waste mass and the presence or absence of migration pathways of LFG and moisture throughout the waste in place (Reddy et al. 2010). Depending on the level of pre-processing of incoming tire materials to the landfill, the compressibility of these materials is likely higher than other MSW waste constituents, such as metals, glass, or other hard plastics. Areas with high quantities of these materials are likely to settle faster in the landfill environment (Edil and Bosscher, 1994, Warith and Rao 2006). However, depending on the degree of post-processing, these materials range from relatively impermeable (whole tires) to permeable (aggregates), that will either inhibit or facilitate LFG and moisture transport through the waste mass, thereby serving as both a source and stymy/accelerator of LFG transfer to the gas collection system. While the liquid permeability of these materials has been well studied, gas transport through waste tire materials has received relatively little attention in the scientific literature.

Even though waste tires can leach a variety of contaminants, waste tires are also well-known adsorbents of NMVOCs and other organic contaminants (Baykal et al. 1992, Park et al. 1996, Edil et al. 2004, Edil 2008). Similar to biodegradation, the sorption capacity of tire materials depends on the state of waste tire processing, ranging from whole tires, to chips, to crumb tire particles. As the active surface area for adsorption increases with a decrease in particle size, greater adsorption of organic contaminants has been documented (Kim et al. 1997). Both adsorption (to the surface) and absorption (phase portioning) affect the physico-chemical attachment of organic contaminants to waste tires (Kim et al. 1997, Alamo-Nole et al. 2012, Hüffer et al. 2020). For example, across a range of organic sorbate materials, absorption into the rubber fraction of the SBR was observed to dominate adsorption onto the black carbon component (Alamo-Nole et al. 2012, Hüffer et al. 2020). Regardless of the exact molecular mechanism governing attachment, multiple studies indicated that waste tires can serve as effective sorbents for leachate quality control in the landfill environment, targeting the removal of polar and non-polar organic chemicals such as benzene, toluene, xylene, ethylbenzene, and other harmful petroleum derived contaminants (Baykal et al. 1992, Park et al. 1996, Edil et al. 2004, Edil 2008). Despite the strong coverage of aqueous contaminant removal by waste tires, few studies have directly quantified the effectiveness of waste tire materials in preventing NMVOC emissions from landfill covers; however, waste tires have been considered for enhancing the gas-phase permeability of soil covers to improve methane oxidation (i.e., biocovers) and to facilitate gas collection (Stern et al. 2007, Jung et al. 2011).

4.10.3 Sulfur Compound and Aromatic Hydrocarbon Emissions

Santa Maria Regional Landfill, Teapot Dome Landfill, Site A Landfill, and Chiquita Canyon Landfill accept waste tires, whereas tires were not accepted at Potrero Hills Landfill. Both Santa Maria Regional and Site A Landfills accepted tire chips or

aggregates only, whereas the other two landfills accepted all types of tire wastes, ranging from whole tires to tire chips and aggregates. Figure 4.92 summarizes the RSC flux measurements as a function tire acceptance. Median RSC fluxes were generally highest for the site that did not accept waste tires (Potrero Hills), followed by Chiquita Canyon, Teapot Dome, Santa Maria Regional and Site A Landfills. The whiskers of each boxplot extended below 0, indicating the probability of net uptake over net emissions. However, as there were many positive outliers and the mean was above the median, measurements were positively skewed, indicating greater probability of RSC emissions over uptake. The variation in RSC flux measurements was generally lowest and highest for Chiquita Canyon and Potrero Hills landfills, respectively as indicated by the IQR and IWR values. The magnitude of the median values was relatively similar across all landfill sites, ranging less than 1 order of magnitude (10^{-5} to 10^{-6}). These results indicate that the presence of tires did not have a significant impact on RSC fluxes and that alternative sources, such as organics present in food or yard waste, contribute to RSC emissions.

Figure 4.92 Summary of Reduced Sulfur Compound Emissions from Landfills with and without Waste Tires by Landfill Site (open black diamonds, red lines, solid red dots represent means, medians, and outliers, respectively).

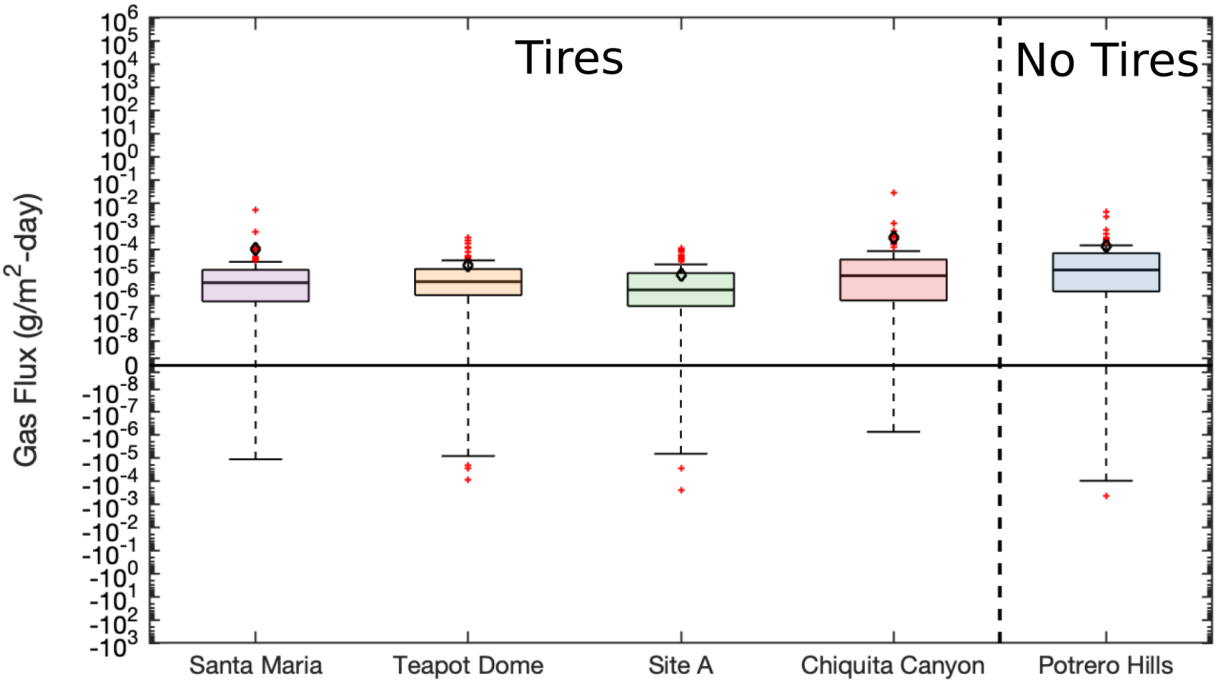

RSC flux measurements are further examined according to cover category for landfills accepting and not accepting waste tires in Figure 4.93. Similar to results presented in Figure 4.92, RSC flux measurements were generally higher for the site that does not accept waste tires based on the median values presented. For both sites accepting and not accepting waste tires, RSC flux measurements were highest from daily cover locations followed by intermediate and final cover locations. Variation in flux measurements as a function of cover category was generally comparable across all cover categories; however, the variation in RSC flux measurements was generally

higher across daily cover locations for sites that did not accept tire wastes (Figure 4.93). The variation in median fluxes between cover categories was within one to two orders of magnitude, indicating that it was difficult to attribute elevated RSC emissions to waste tires alone. Sulfur reducing bacteria may use substrates present in other organic wastes such as food (i.e., decaying meats or dairy products) or green/yard wastes (i.e., fertilizers, manures, treated sewage sludge that lead to the production of RSC.

Figure 4.93 Summary of Reduced Sulfur Compound Emissions from Landfills with and without Waste Tires by Cover Category (open black diamonds, red lines, solid red dots represent means, medians, and outliers, respectively).

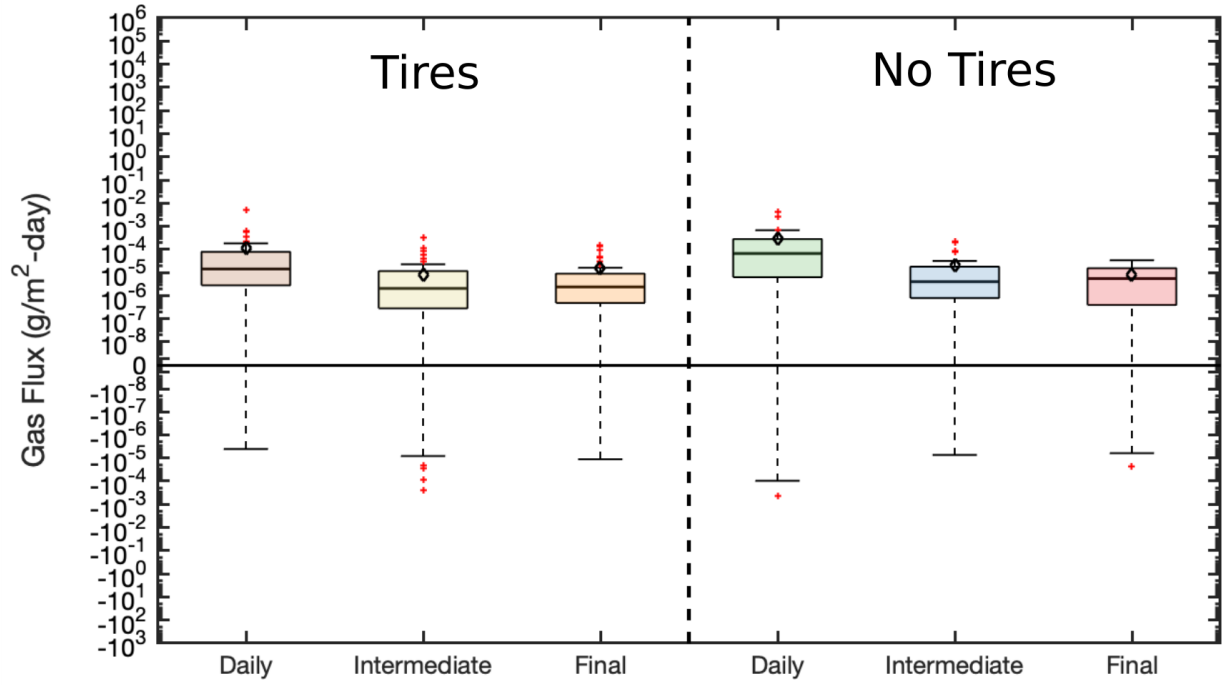

Figure 4.94 summarizes the aromatic compound flux measurements as a function tire acceptance. Aromatic compound fluxes including median flux were generally higher for the site that did not accept waste tires (Potrero Hills). As introduced in 4.10.2 above, waste tires have high sorption potential for aromatic hydrocarbons (i.e., benzene, toluene, xylene, ethylbenzene). Santa Maria Regional Landfill and Site A Landfill had the lowest median Ar fluxes including net uptake at Site A Landfill. These low fluxes likely resulted from the small size and thus large surface area of the form of tires, tire chips and aggregates, accepted at these two sites. The Ar fluxes at Teapot Dome Landfill and Chiquita Canyon Landfill were higher than Santa Maria Regional and Site A Landfills likely due to the large size and thus low surface area of the whole tires accepted at these sites.

Figure 4.95 compares aromatic compound emissions from sites accepting and not accepting waste tires as a function of cover category. In general, Ar fluxes from daily covers at sites not accepting waste tires were greater than fluxes observed from sites accepting waste tires, whereas fluxes from intermediate and final covers were relatively comparable but slightly greater for sites accepting waste tires (Figure 4.95).

These results confirm trends observed above that the presence of waste tires are potentially sorption sites retarding the transport of Ar compounds as they travel through the waste mass.

Figure 4.94 Summary of Aromatic Compound Emissions from Landfills with and without Waste Tires by Landfill Site (open black diamonds, red lines, solid red dots represent means, medians, and outliers, respectively).

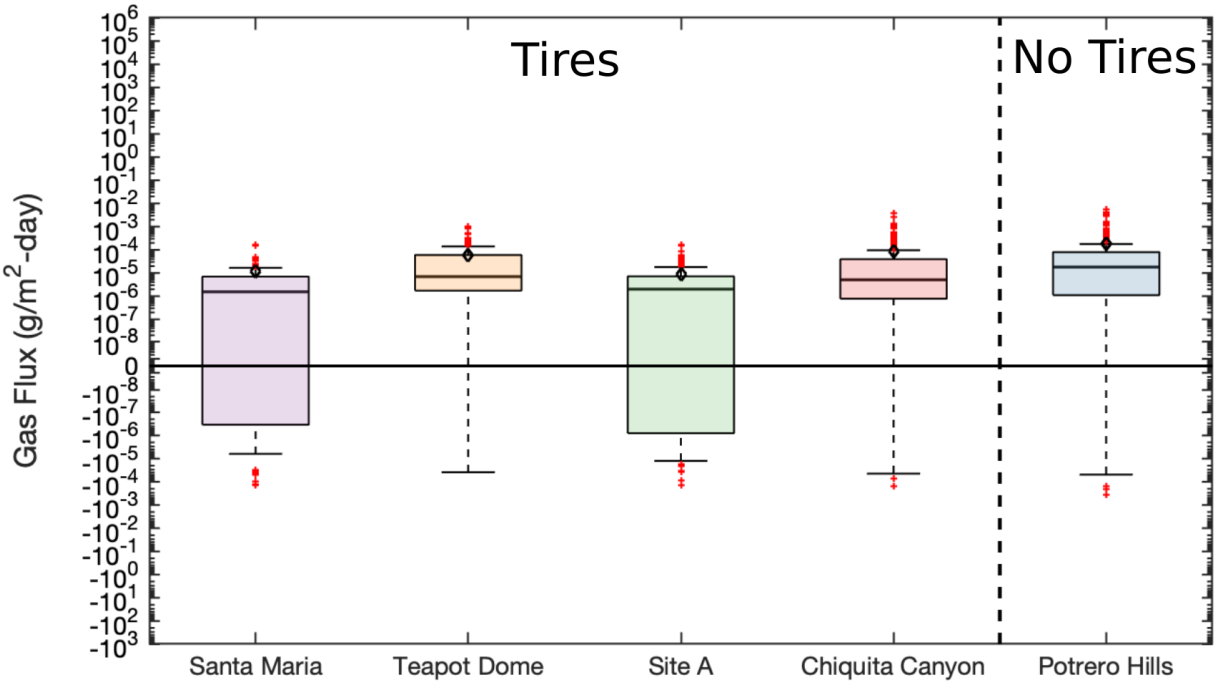

Figure 4.95 Summary of Aromatic Compound Emissions from Landfills with and without Waste Tires by Cover Category (open black diamonds, red lines, solid red dots represent means, medians, and outliers, respectively).

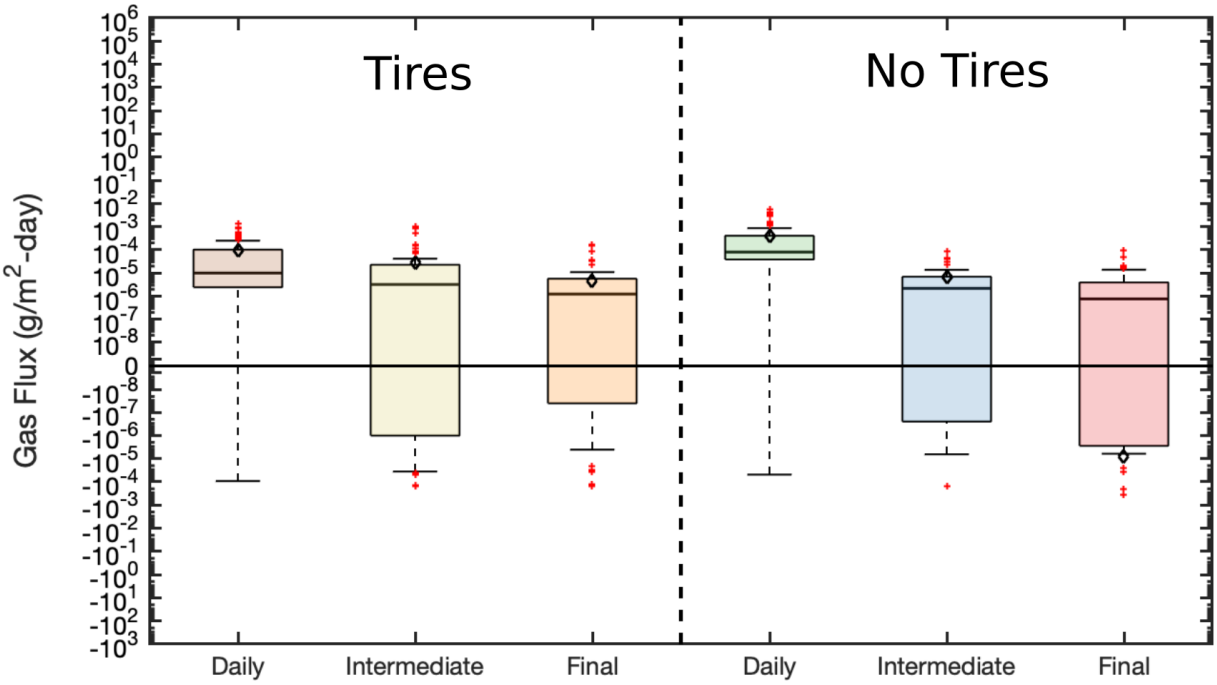

The overall methane, RSC, and Ar fluxes for all sites accepting and not accepting tires are compared in Figure 4.96. Methane fluxes were generally higher from waste sites that do not accept tires, as indicated by the median flux values in the box plots (Figure 4.96). Moreover, RSC and Ar fluxes were slightly higher, on average, for sites not accepting waste tires as compared to sites accepting waste tires (Figure 4.96). There was a higher probability of net uptake over emissions for methane as compared to the RSCs and Ars across all landfills and cover systems investigated (Figure 4.96). The variation in both methane, RSC, and Ar flux measurements was greater for sites not accepting tire wastes given the lengths of the IQR and IWR of the boxplots. Therefore, these results suggest that the presence of tire waste may impede migration of LFG to the base of the cover, thus influencing emissions. However, since there is no way to reliably evaluate both generation and migration of these gases in the landfill environment, it is difficult to make any definitive conclusions about how gas transport is affected in the waste mass by the presence of waste tire materials. Moreover, it is difficult to ascertain the sources of both RSC emissions, as sulfur-reducing bacteria may use substrates present in other organic wastes such as food (i.e., decaying meats or dairy products) or green/yard wastes (i.e., fertilizers, manures, treated sewage sludge). The sources of Ar compounds, however, are primarily anthropogenic, where differences in emissions may be attributed to both generation, sorptive, and perhaps biodegradative processes occurring within the different landfills.

Figure 4.96 Summary of Methane and Reduced Sulfur Compound Emissions from Landfills with and without Waste Tires (open black diamonds, red lines, solid red dots represent means, medians, and outliers, respectively).

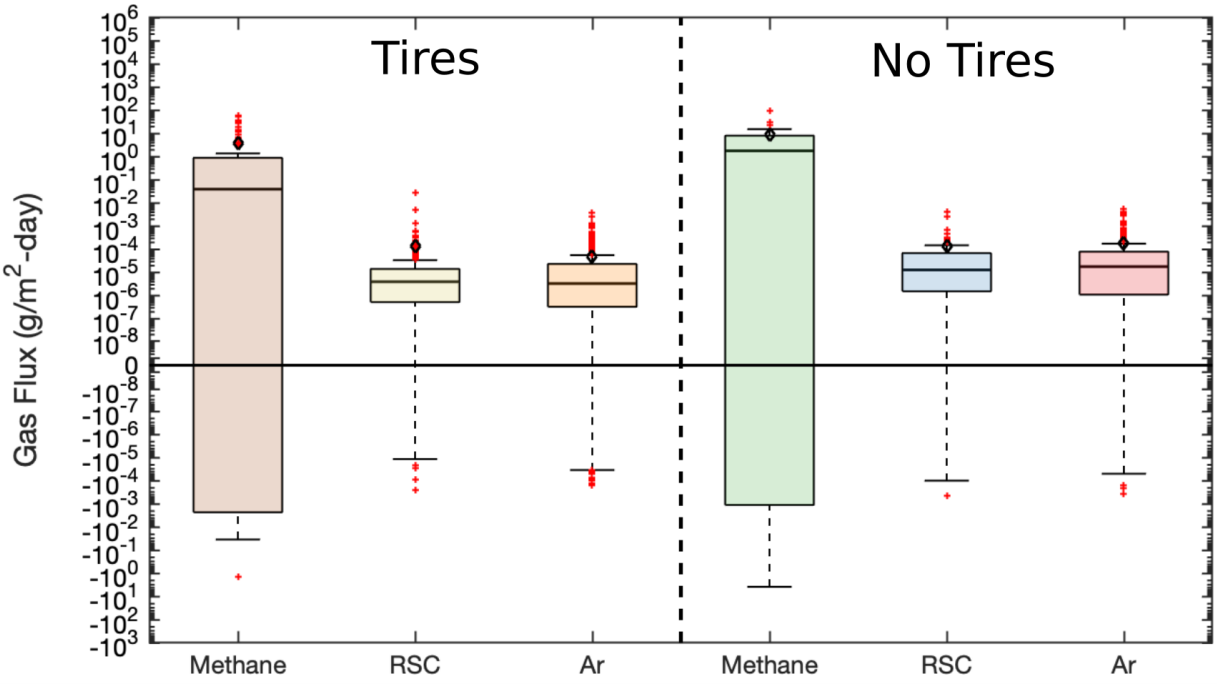

A two-sample t-test (significance level of 0.05, two tails, unequal variance) was conducted to ascertain whether the differences in methane, RSC, and Ar fluxes observed above between sites accepting and not accepting waste tires were in fact statistically significant. A conservative approach using both tails of the normal distributions, unequal variances, and a significance level of 0.05 was applied. Using these assumptions, the null hypothesis is that the distributions of fluxes for a given chemical family between sites accepting/not accepting waste tires come from independent random samples from normal distributions with equal means and unequal but unknown variances. The results of this two-sample t-test are summarized in Table 4.28 below. Statistically significant differences in the fluxes of the aromatic compounds were observed between sites accepting and not accepting waste tires as the p-value was below the significance level of 0.05 (Table 4.28). These results provide further confidence that the presence of waste tires affect the transport and transformation of aromatic compounds in the landfill environment. However, statistically significant differences were not observed for both methane and RSC fluxes between sites accepting and not accepting waste tires, indicating that there is less confidence in the initial presumption that RSC generation and overall LFG transport/transformation are affected by the presence of waste tires. The conclusions presented herein may be affected, to some degree, by differences in the sample sizes of the flux distributions under comparison (4 sites vs. 1 site), where additional data from landfill sites not accepting waste tires would provide a more balanced comparison of the potential effect of waste tires on LFG generation, transport/transformation, and emissions.

Table 4.30 – Summary of t-Test Results for Sites Accepting and Not Accepting Waste Tires

Chemical Family	Accept or Reject?	p-values
Methane	Accept	0.246
RSC	Accept	0.985
Ar	Reject	5.29E-4

4.11 Raw Gas Tests

Concentration data are provided for gases sampled prior to the inlet of the flare and/or gas to energy systems at the five landfills included in the ground-based flux investigation. The composition of these samples represents the composition of gas in the waste mass, unaffected by transformation processes occurring in the cover soils. The concentration data for the raw gas are presented as a function of chemical family and site in Figures 4.97 and 4.98, respectively. Highest LFG concentrations were obtained for the GHGs, with median values ranging from 20,000 to 100,000 μg/L. Concentrations of the remaining NMVOCs were significantly lower, on the order of 10^{-4} to 500 μg/L. Based on median concentration values, the alcohols, ketones, monoterpenes, and alkanes had the highest concentrations. Organic alkyl nitrates (ON) were not detected in LFG. The differences between seasonal results were minimal (Figure 4.97). Among the NMVOC families, the F-gases and the monoterpenes had the highest variation in the dry and wet seasons, respectively.

Figure 4.97 LFG Concentrations Measured in the a) Dry and b) Wet Seasons by Chemical Family (open black diamonds, black lines, solid red dots represent means, medians, and outliers, respectively).

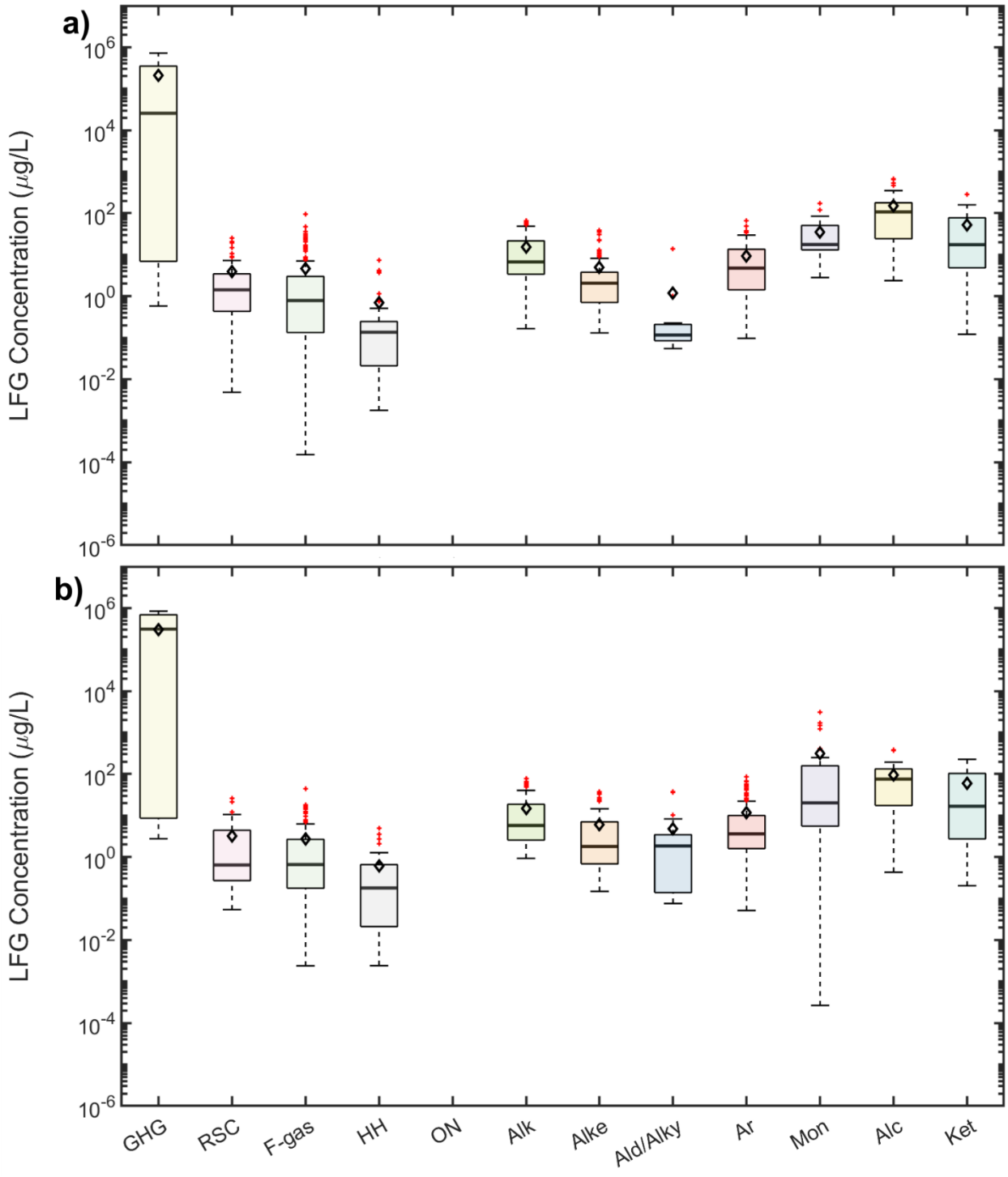

Figure 4.98 summarizes the LFG concentrations as a function of landfill site, where results are presented for methane, nitrous oxide, carbon dioxide, carbon monoxide, and total NMVOCs. LFG concentrations were similar between the sites with the median LFG

concentrations varying less than one to two orders of magnitude. The only exception to this trend was observed for carbon dioxide, where the CO_2 concentrations at Santa Maria Regional Landfill were generally lower than the remaining landfills included in this study (Figure 4.98). Concentrations of the specific gas constituents were generally highest at Site A Landfill and lowest at Santa Maria Regional Landfill. NMVOC concentrations were generally relatively similar across the sites investigated. The mean NMVOC concentrations were higher than the median values calculated. The low differences in LFG concentrations observed between the landfill sites suggest that the waste composition, landfill conditions, and LFG generation mechanisms are relatively similar across the landfills studied, regardless of the differences in operational scale and practice.

Figure 4.98 GHG and NMVOC LFG Concentrations as a Function of Landfill Site (open black diamonds, red lines, solid red dots represent means, medians, and outliers, respectively).

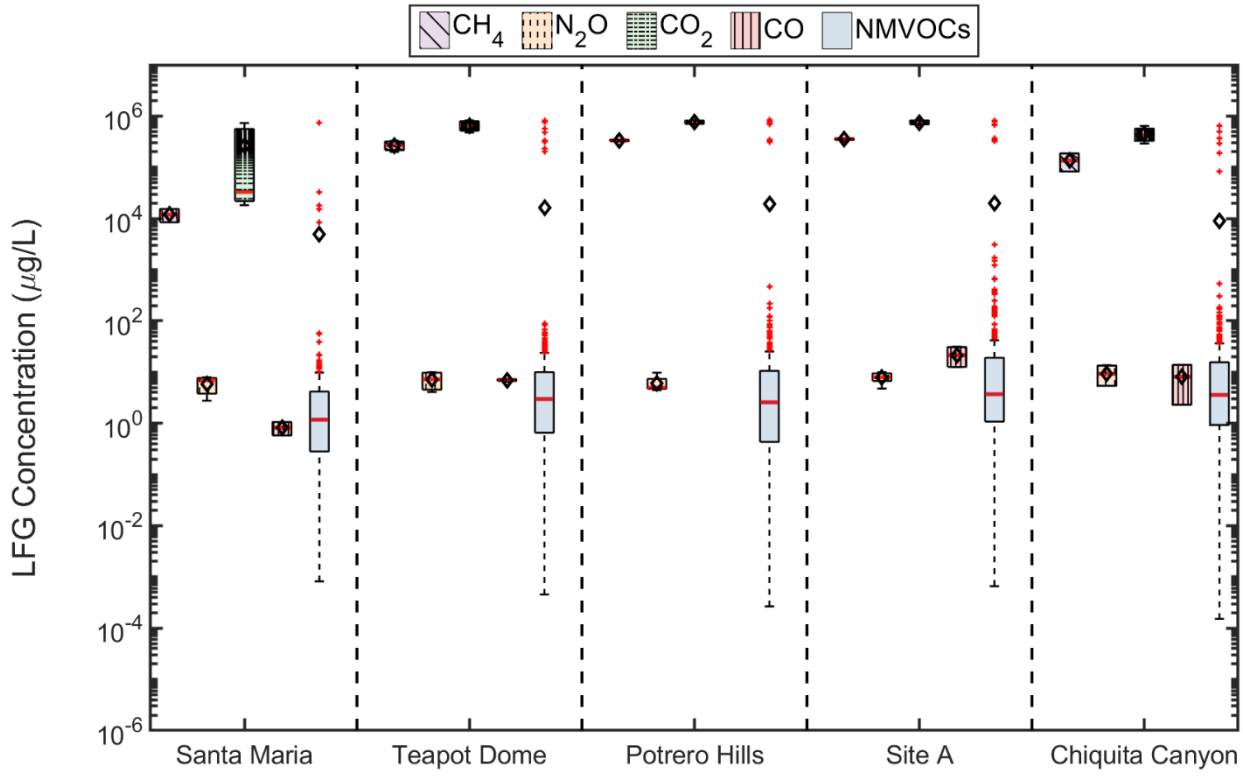

Measured LFG concentrations are compared to ambient LFG concentrations in Figure 4.99. Ambient concentrations were established using the initial (time = 0) concentration datapoints in the flux chamber tests. The raw LFG concentrations were significantly (two to over five orders of magnitude) higher than the ambient concentrations based on differences in median concentrations. The lowest differences were observed for the GHGs. Similar to raw gas data (Figure 4.97), the alcohols, ketones, and alkanes were had the highest ambient concentrations. The organic alkyl nitrates were present in the ambient air at each landfill site (Figure 4.99), yet these chemicals were not detected in

raw gas (Figure 4.97), suggesting potential generation occurring within the cover materials.

Figure 4.99 LFG (darker shading) and Ambient (lighter shading) Concentrations Measured in the a) Dry and b) Wet Seasons by Chemical Family (open black diamonds, black lines, solid red dots represent means, medians, and outliers, respectively).

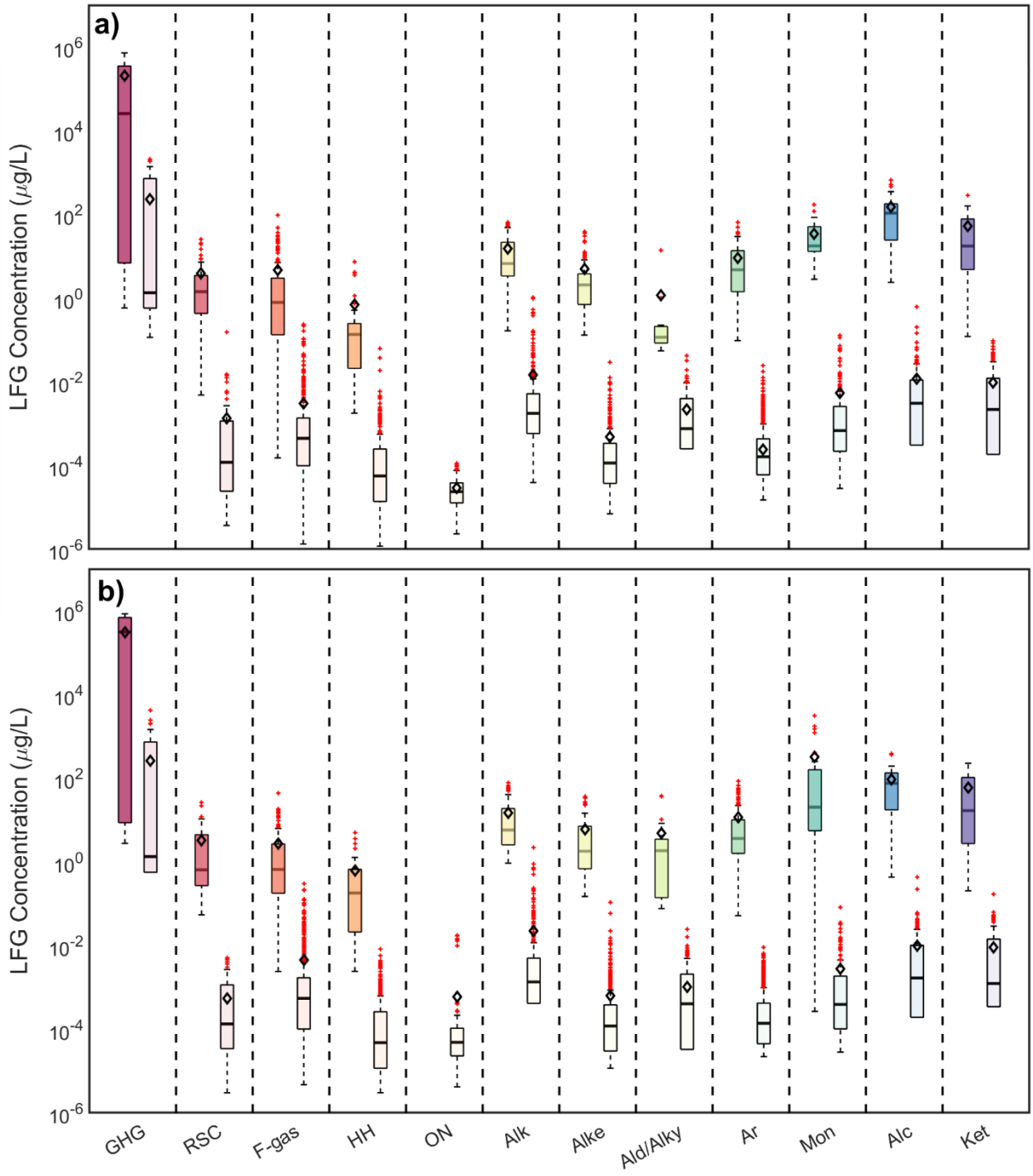

4.12 Temperature Conditions in Covers

Temperatures were measured to determine temperature in tested covers near the ground surface (150 mm depth) at time of testing within each chamber footprint. Also, temperatures were measured with depth at a selected cover location for each of the 5 ground-based testing landfills over seasonal durations. At time of testing, average near-surface temperatures ranged from 10 to 56 °C. Example temperature-time data is presented in Figure 4.100 for Santa Maria Regional Landfill for July 2018 to October 2019. Temperatures are presented for 10, 20, 40, and 80 mm below the ground surface. Maximum and minimum daily air temperatures are also presented. High diurnal variation in temperatures is observed at the shallow depths. This high frequency fluctuation is dampened with depth to where virtually no diurnal fluctuation is present at 40 mm depth. The seasonal variations in temperature are affected by depth with both phase lag (i.e., delay in seasonal peaks) and amplitude decrement (i.e., smaller range of temperatures over seasonal cycles) occurring within the depth of the cover system.

Figure 4.100 Temperature with Time for Various Depths through Interim Cover System at Santa Maria Regional Landfill

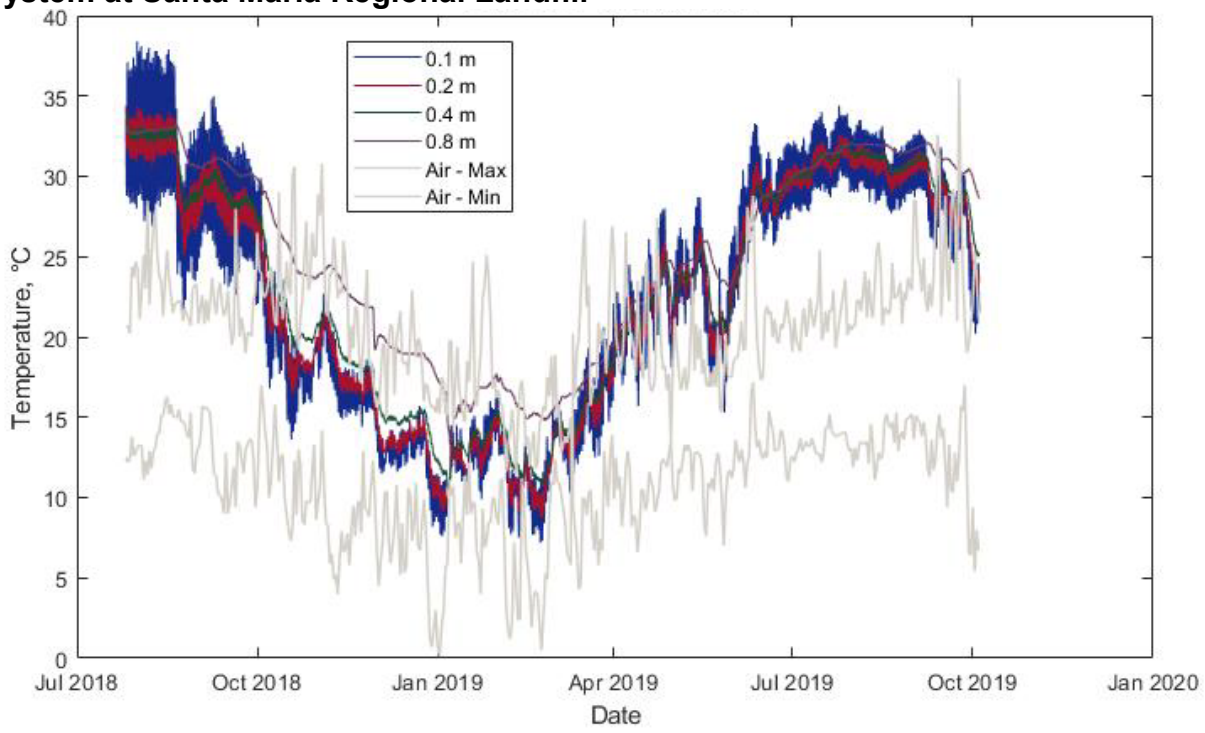

Temperature with depth profiles for the same cover system (and same timeline) are presented in Figure 4.101. All data at each measurement depth are presented to produce an envelope of temperature variation with depth. The seasonal amplitude decrement is present in this plotting domain. Seasonal temperature fluctuation is greatest near the ground surface and decreases with depth. Similar analysis of temperatures was conducted for each of the 5 sites. The range of minimum to maximum temperatures at 10 mm depth over the periods of measurement were 7.2 to

38.4°C for Santa Maria Landfill, 7.6 to 43.4°C for Teapot Dome Landfill, 5.9 to 36.2°C for Potrero Hills Landfill, 7.1 to 39.4°C for Site A Landfill, and 8.3 to 46.3°C for Chiquita Canyon Landfill. The high temperatures in the cover systems (exceeding maximum air temperatures) were partly attributed to warming caused by underlying waste mass (Yesiller et al. 2008). The particularly high temperatures at Chiquita Canyon were attributed to a on old green waste cover (placed for erosion control purposes) overlying interim soil cover.

Figure 4.101 Temperature Variation with Depth for Thermocouple Array within Interim Cover System at Santa Maria Regional Landfill

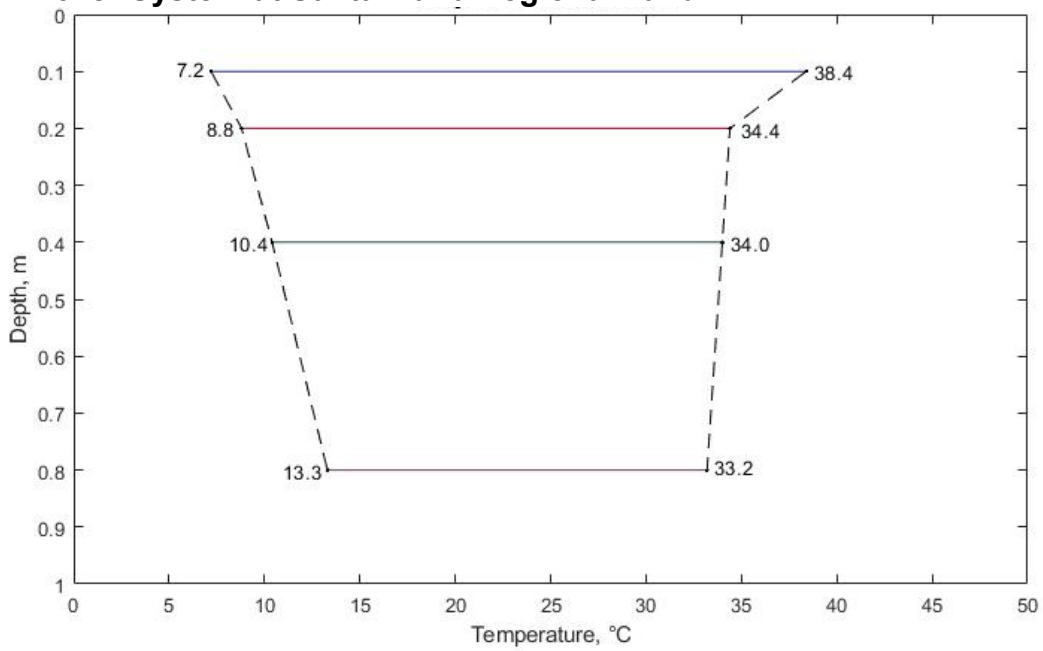

4.13 Additional Static Flux Chamber Investigations

4.13.1 Radial Gas Well Testing Results at SMRL

Figures 4.101 and 4.102 summarize the trends in overall fluxes as a function of the radial distance from the well for both test days. The measured surface flux of the GHGs, both median and mean values, generally increased progressing from near-well locations (0.5 and 1 m radial distance) to the far-field test locations (16 and 32 m radial distance). Negative median GHG fluxes were observed in close proximity of the extraction well on Test Day 1. The variation in GHG fluxes at a given testing location was higher than the variations in NMVOC fluxes at a given location. In general, variations in GHG fluxes with distance from the well was higher than the variations in NMVOC fluxes with distance from the extraction well (Figures 4.101 and 4.102). Overall, the variations in flux with radial distance was detectable, yet relatively low for analysis using directly measured flux data.

Figure 4.102 Influence of Radial Well Distance on a) GHG and b) NMVOC Fluxes at SMRL (Test Day 1).

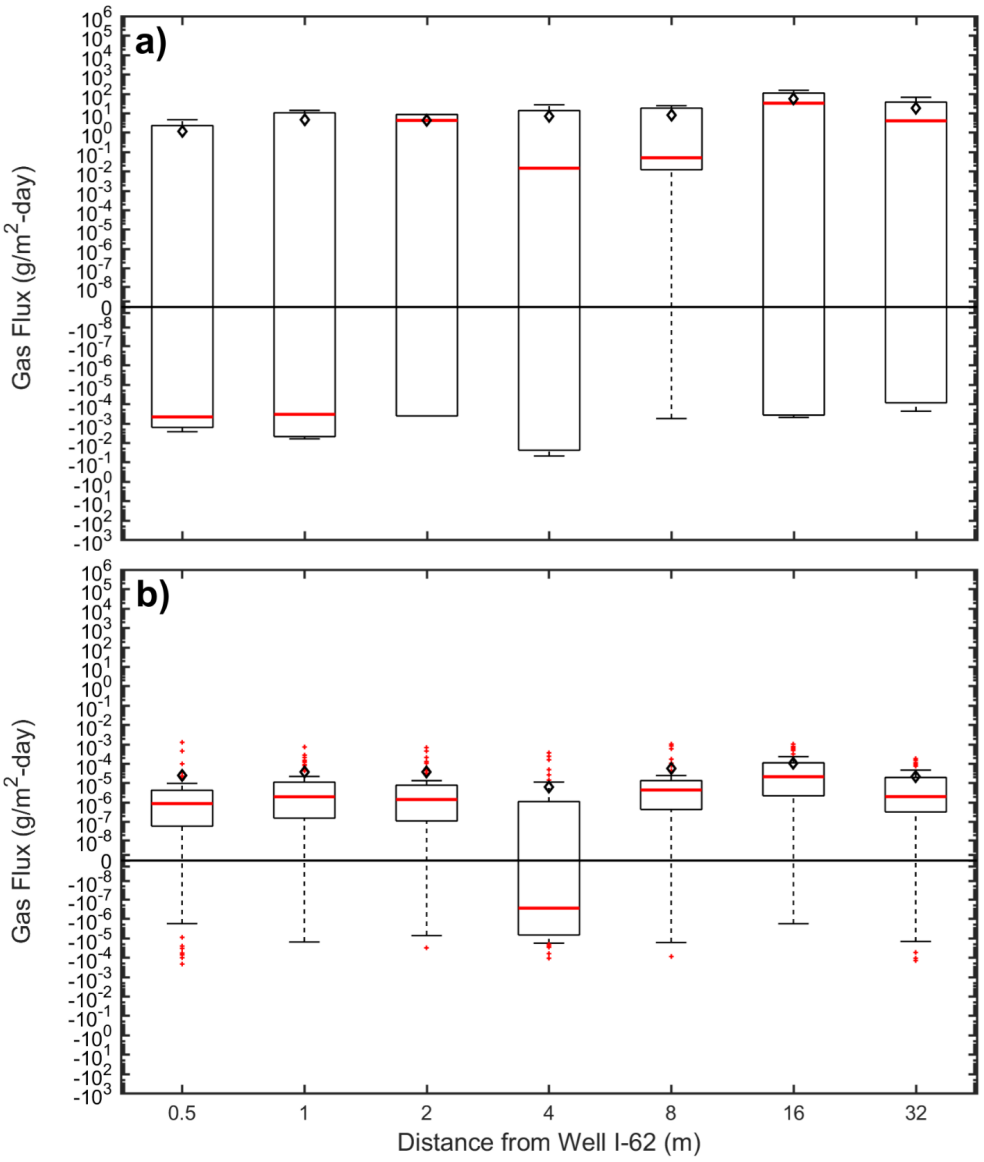

Figure 4.103 Influence of Radial Well Distance on a) GHG and b) NMVOC Fluxes at SMRL (Test Day 2).

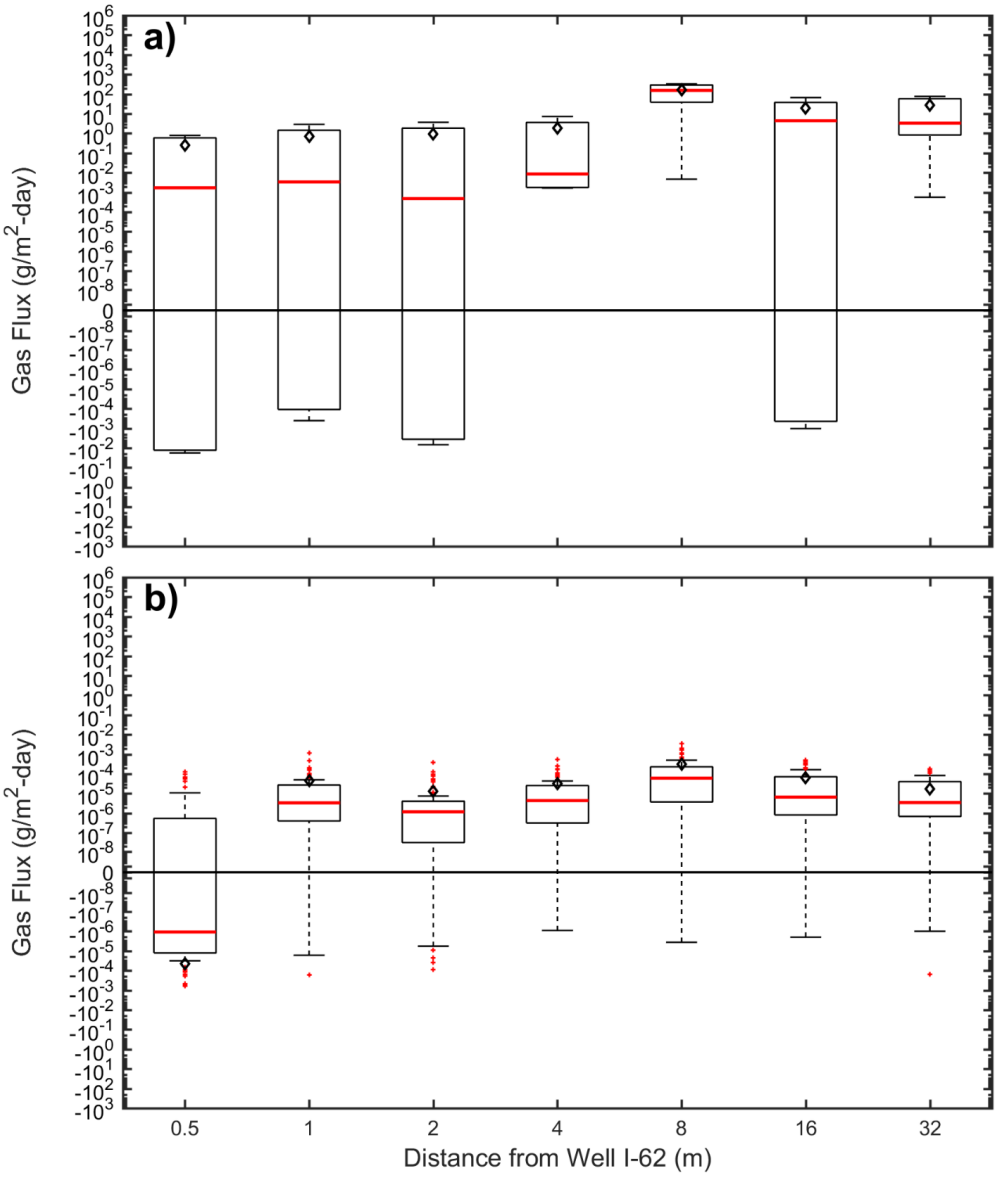

Vacuum pressures of the gas extraction system measured over the two test days are presented in Figure 4.103. During Chamber 3 and 4 tests on both days, the vacuum pressure declined significantly. Variations in cover thickness during the radial well distance tests are presented in Table 4.27. The cover thickness decreased significantly progressing from the near well locations to the farthest test location at 32 m away from the well. High cover thicknesses are used near extraction wells at SMRL to minimize potential intrusion of atmospheric air and fugitive emissions at locations near the annular space of the wells.

Figure 4.104 Variation in Vacuum Pressure Monitored at Well I-62 (shallow) and I-62A (deep) for a) Test Day 1 and b) Test Day 2.

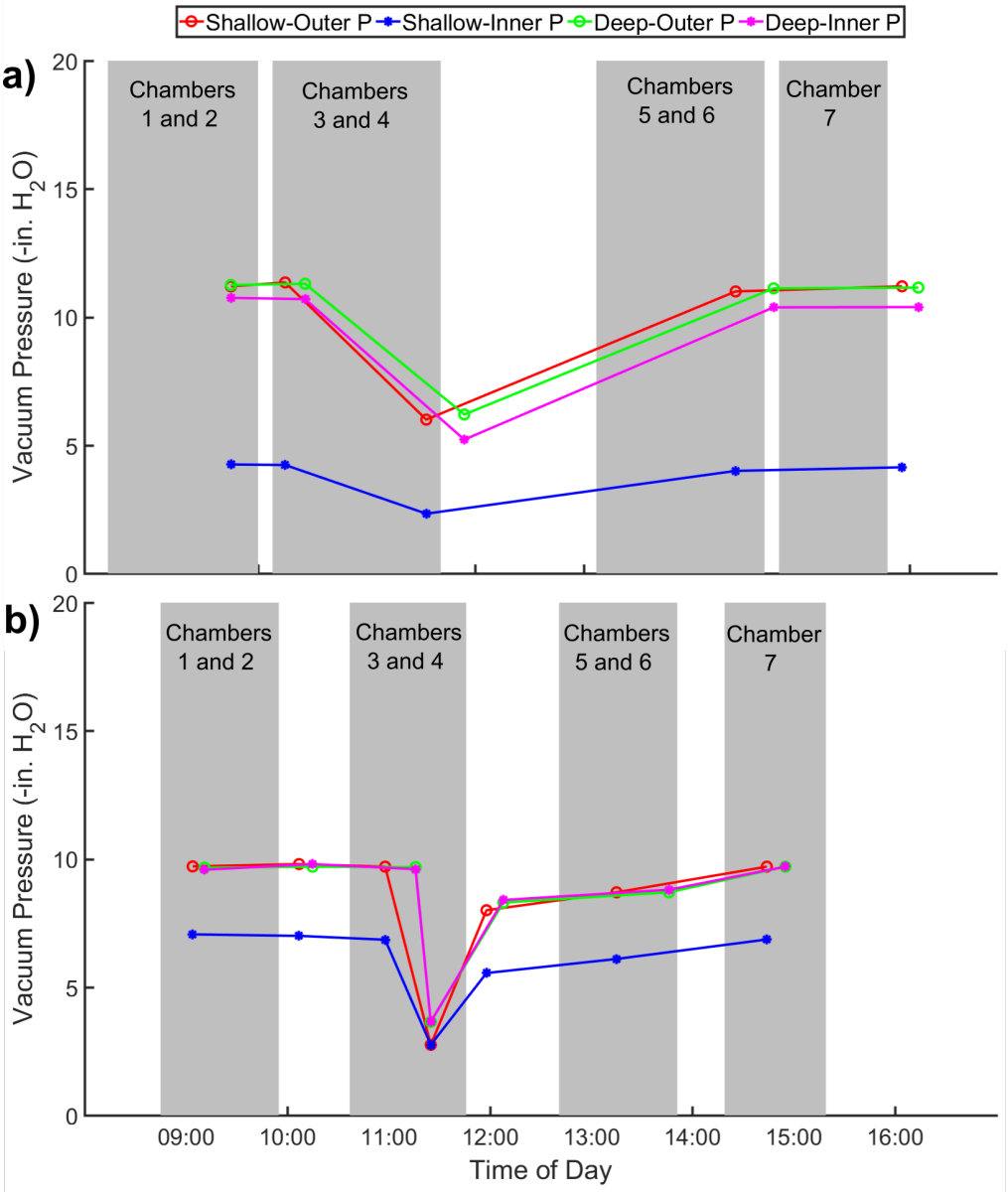

Table 4.31 – Variation in Cover Thickness as a Function of Radial Distance

Chamber Number	Radial Distance (m)	Cover Thickness (cm)
Chamber 1	0.5	125
Chamber 7	1	125
Chamber 2	2	125
Chamber 3	4	109-110
Chamber 4	8	101-102
Chamber 6	16	77-78
Chamber 5	32	61-62

The measured fluxes were adjusted using the vacuum pressure and cover thickness data to analyze variation of flux solely with radial distance without the effects of varying pressure during the tests as well as the varying cover thicknesses at the different measurement locations. Adjustment factors were calculated both for pressure and thickness using the relative ratio of the pressure or thickness at a given location to the maximum pressure and maximum thickness obtained in the investigation, respectively. The measured flux increased with decreasing pressure and decreasing thickness. Measured and adjusted flux data for GHGs and NMVOCs are presented in Tables 4.28 and 4.29, respectively. The adjusted fluxes are presented in Figures 4.104 and 4.105 for Test Days 1 and 2, respectively. The variations between the fluxes with radial distance increased modestly due to the applied adjustment. The adjusted GHG emissions increased from the near-well locations to the far-field test locations with somewhat more variation observed for median fluxes than mean fluxes, in particular for Test Day 1. Similarly, the adjusted NMVOC emissions increased from the near-well locations to the far-field locations with somewhat more variation observed for median fluxes than mean fluxes.

Table 4.32 – Variation in Radial Distance Fluxes for Measured and Adjusted Data (Testing Day 1)

Radial Distance (m)	Measured Mean GHG Flux (g/m^2-day)	ΔP Adjusted Mean GHG Flux (g/m^2-day)	ΔT Adjusted Mean GHG Flux (g/m^2-day)	ΔP+ΔT Adjusted Mean GHG Flux (g/m^2-day)	Measured Median GHG Flux (g/m^2-day)	ΔP Adjusted Median GHG Flux (g/m^2-day)	ΔT Adjusted Median GHG Flux (g/m^2-day)	ΔP+ΔT Adjusted Median GHG Flux (g/m^2-day)
0.5	$1.14x10^{0}$	$1.14x10^{0}$	$1.14x10^{0}$	$-4.68x10^{-4}$	$-4.68x10^{-4}$	$-4.68x10^{-4}$	$-4.68x10^{-4}$	$-4.68x10^{-4}$
1	$4.60x10^{0}$	$4.62x10^{0}$	$4.60x10^{0}$	$-3.42x10^{-4}$	$-3.42x10^{-4}$	$-3.44x10^{-4}$	$-3.42x10^{-4}$	$-3.44x10^{-4}$
2	$4.21x10^{0}$	$4.21x10^{0}$	$4.21x10^{0}$	$4.21x10^{0}$	$4.21x10^{0}$	$4.21x10^{0}$	$4.21 x10^{0}$	$4.21 x10^{0}$
4	$6.72x10^{0}$	$9.79x10^{0}$	$7.55x10^{0}$	$1.61x10^{-2}$	$1.44x10^{-2}$	$2.09x10^{-2}$	$1.61 x10^{-2}$	$2.35 x10^{-2}$
8	$8.03x10^{0}$	$1.17x10^{1}$	$9.54x10^{0}$	$5.87x10^{-2}$	$4.94x10^{-2}$	$7.19x10^{-2}$	$5.87 x10^{-2}$	$8.54 x10^{-2}$
16	$5.38x10^{1}$	$5.46x10^{1}$	$7.43x10^{1}$	$4.48x10^{1}$	$3.25x10^{1}$	$3.30x10^{1}$	$4.48x10^{1}$	$4.55x10^{1}$
32	$1.84x10^{1}$	$1.87x10^{1}$	$2.78x10^{1}$	$6.04x10^{0}$	$4.01x10^{0}$	$4.07x10^{0}$	$6.04x10^{0}$	$6.13x10^{0}$

Table 4.33 – Variation in Radial NMVOC Fluxes for Measured and Adjusted Data (Testing Day 1)

Radial Distance (m)	Measured NMVOC Flux (g/m^2-day)	ΔP Adjusted NMVOC Flux (g/m^2-day)	ΔT Adjusted NMVOC Flux (g/m^2-day)	ΔP+ΔT Adjusted Mean NMVOC Flux (g/m^2-day)	Measured Median NMVOC Flux (g/m^2-day)	ΔP Adjusted Median NMVOC Flux (g/m^2-day)	ΔT Adjusted Median NMVOC Flux (g/m^2-day)	ΔP+ΔT Adjusted Median NMVOC Flux (g/m^2-day)
0.5	$2.39x10^{-5}$	$2.39x10^{-5}$	$2.39x10^{-5}$	$2.39x10^{-5}$	$8.61x10^{-7}$	$8.61x10^{-7}$	$8.61x10^{-7}$	$8.61x10^{-7}$
1	$3.61x10^{-5}$	$3.63x10^{-5}$	$3.61x10^{-5}$	$3.63x10^{-5}$	$1.93x10^{-6}$	$1.94x10^{-6}$	$1.93x10^{-6}$	$1.94x10^{-6}$
2	$3.79x10^{-5}$	$3.79x10^{-5}$	$3.7x10^{-5}$	$3.79x10^{-5}$	$1.39x10^{-6}$	$1.39x10^{-6}$	$1.39x10^{-6}$	$1.39x10^{-6}$
4	$6.24x10^{-6}$	$9.10x10^{-6}$	$7.02 x10^{-6}$	$1.02x10^{-5}$	$-2.84x10^{-7}$	$-4.14x10^{-7}$	$-3.20x10^{-7}$	$-4.66x10^{-7}$
8	$5.64x10^{-5}$	$8.21x10^{-5}$	$6.70x10^{-5}$	$9.75x10^{-5}$	$4.36x10^{-6}$	$6.35x10^{-6}$	$5.18x10^{-6}$	$7.54x10^{-6}$
16	$1.04x10^{-4}$	$1.06x10^{-4}$	$1.44x10^{-4}$	$1.46x10^{-4}$	$2.11x10^{-5}$	$2.14x10^{-5}$	$2.91x10^{-5}$	$2.95x10^{-5}$
32	$2.15x10^{-5}$	$2.18x10^{-5}$	$3.24x10^{-5}$	$3.28x10^{-5}$	$1.97x10^{-6}$	$2.00x10^{-6}$	$2.97x10^{-6}$	$3.01x10^{-6}$

Figure 4.105 Adjusted Radial Flux Data for a) GHG and b) NMVOC Fluxes at SMRL (Test Day 1).

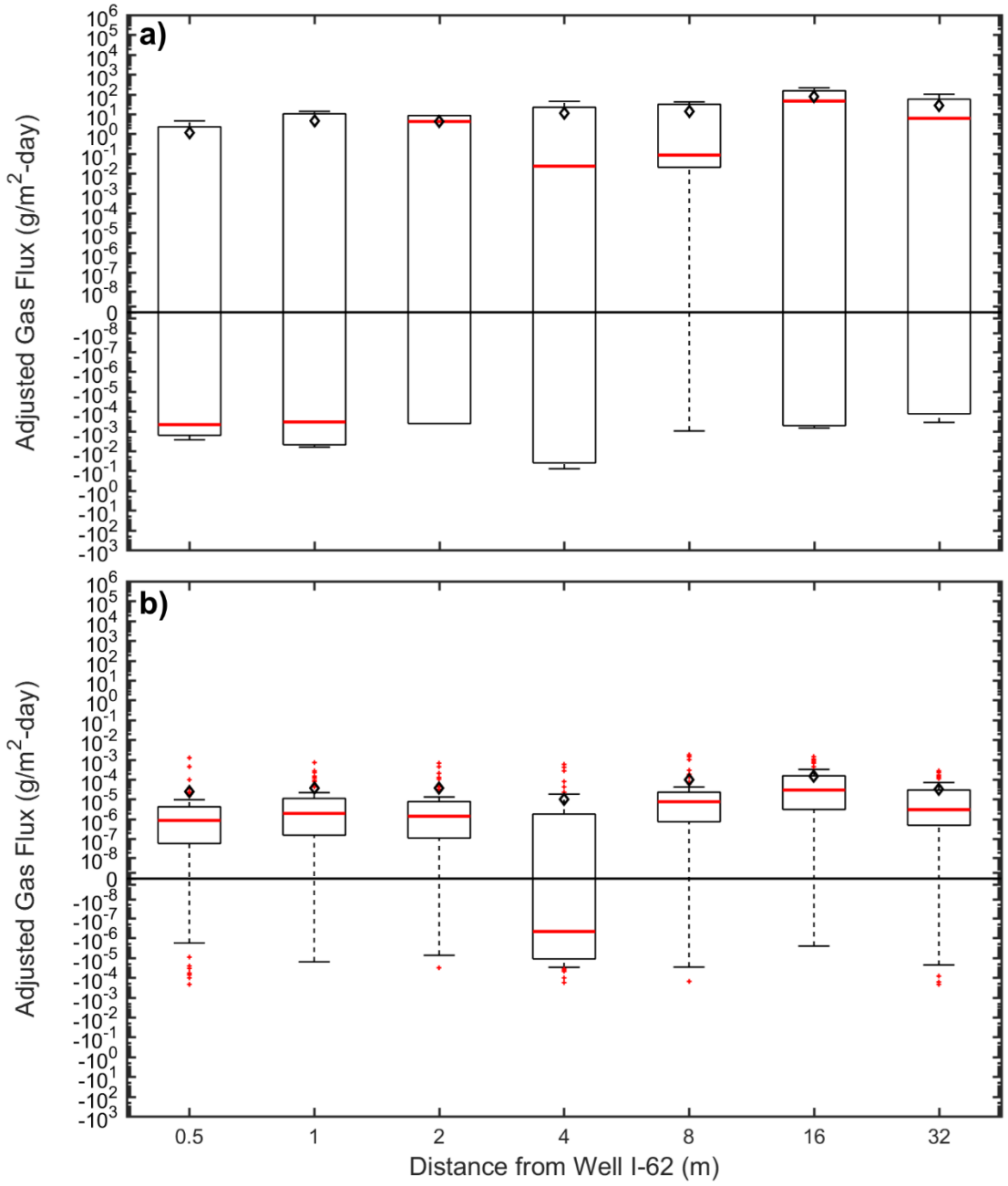

Figure 4.106 Measured and Adjusted Radial Flux Data for a) GHG and b) NMVOC Fluxes at SMRL (Test Day 1).

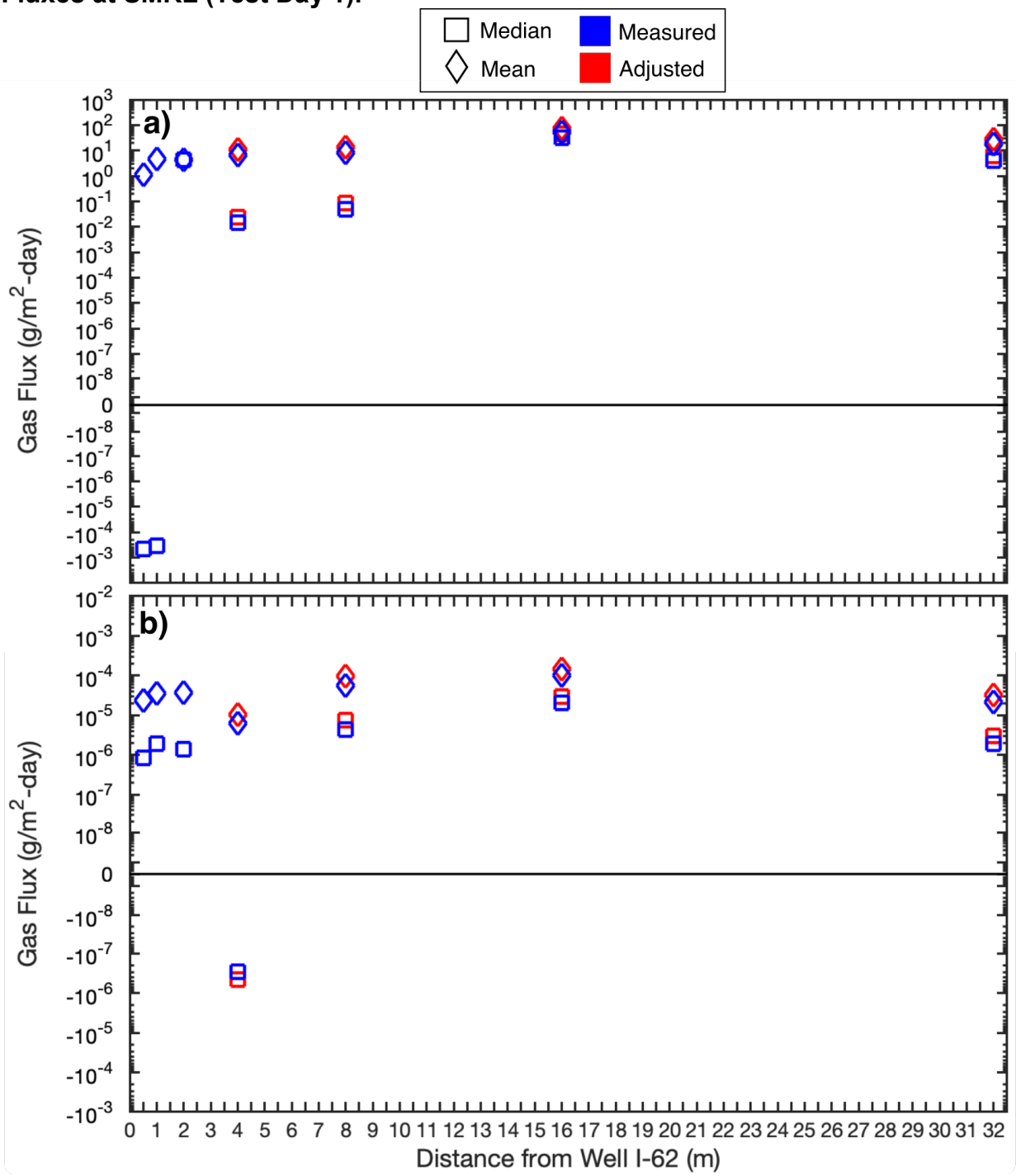

Figure 4.107 Adjusted Radial Flux Data for a) GHG and b) NMVOC Fluxes at SMRL (Test Day 2).

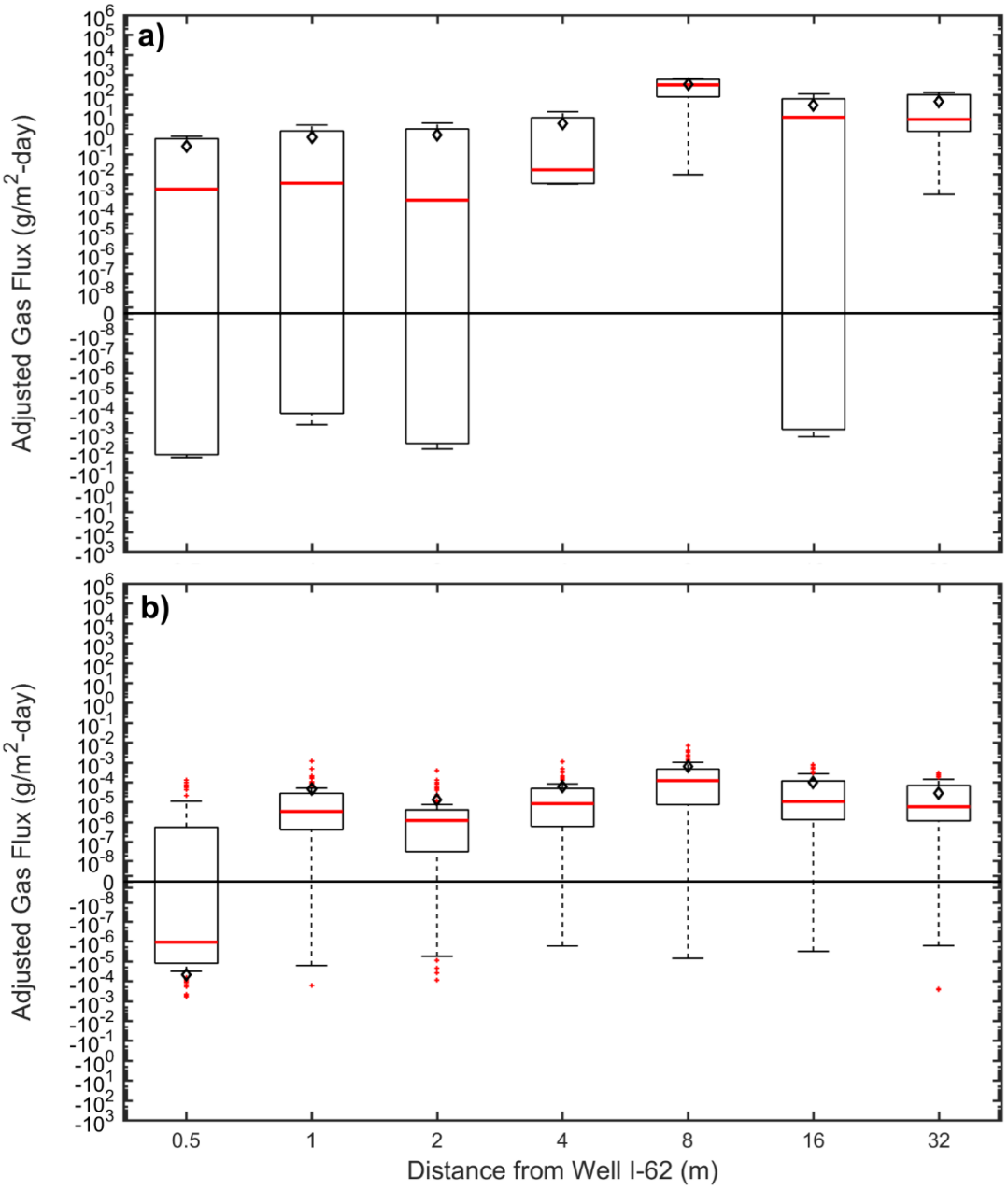

4.13.2 Cover Thickness Testing Results at SMRL

The results of the cover thickness field investigation are presented in Figure 4.107. The median GHG fluxes increased significantly as the intermediate cover thickness decreased from 1.2 m to 0.9 m. For the cover thickness of 1.2 m, the median GHG flux was negative, indicating net uptake from the atmosphere over emissions to the atmosphere, whereas the median GHG fluxes were positive for all lower thicknesses. The average fluxes were all positive and the variation between average GHG fluxes were low between the different thickness measurements. The variation of NMVOC

fluxes was low for a given cover thickness and the variation in NMVOC fluxes between different cover thicknesses also was relatively low, with the lowest NMVOC fluxes observed for the 1.2 m cover thickness.

Figure 4.108 Influence of Cover Thickness on a) GHG and b) NMVOC Fluxes at SMRL.

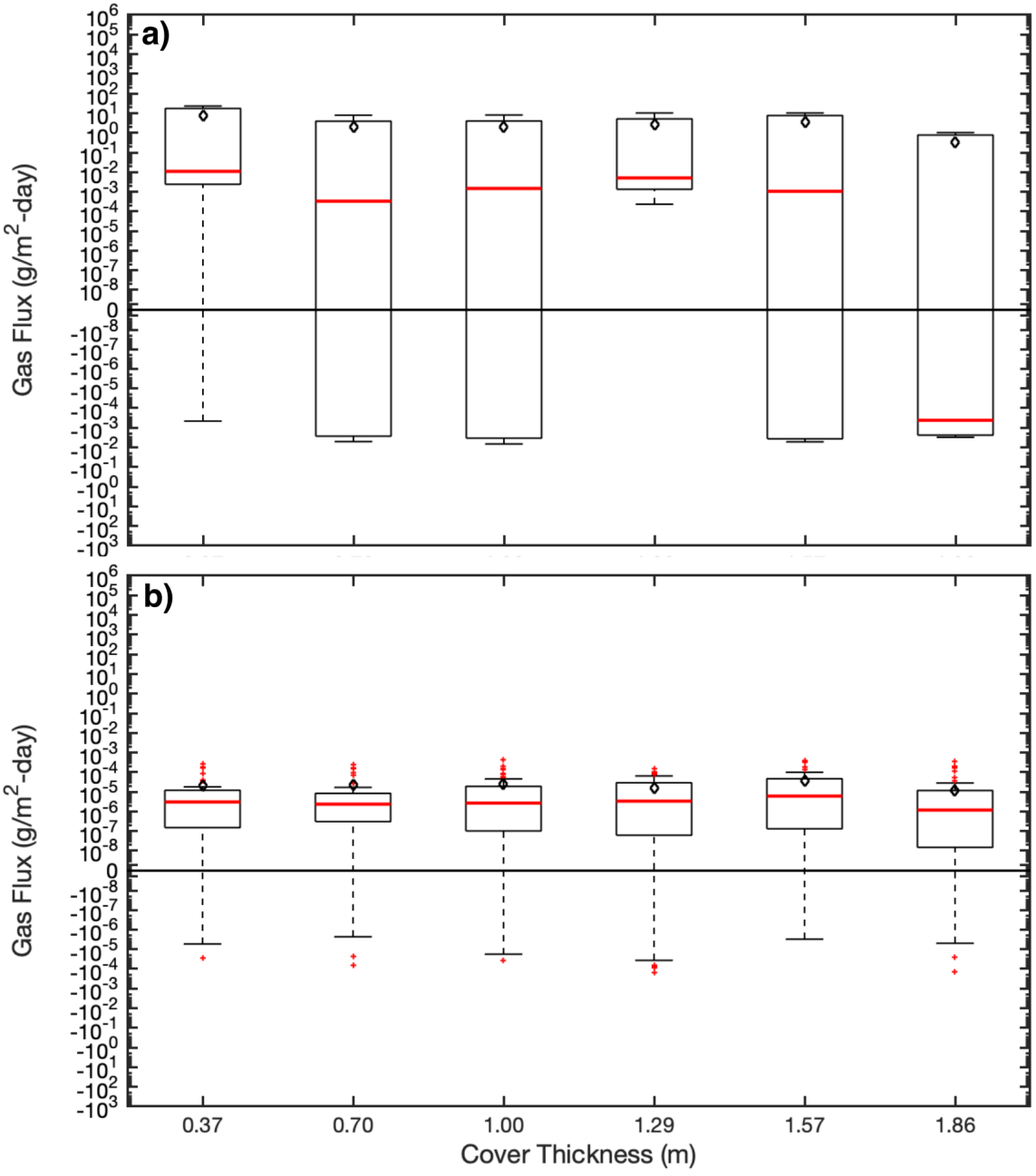

Vacuum pressures of the gas extraction system measured during the thickness tests are presented in Figure 4.108. The pressure was observed to decrease significantly during the 0.61-m cover thickness tests. The pressure was relatively steady during the remaining five thickness tests.

Figure 4.109 Variation in Vacuum Pressure Monitored at Well I-39 (shallow) and I-39A (deep) for the Cover Thickness Testing Program at the SMRL.

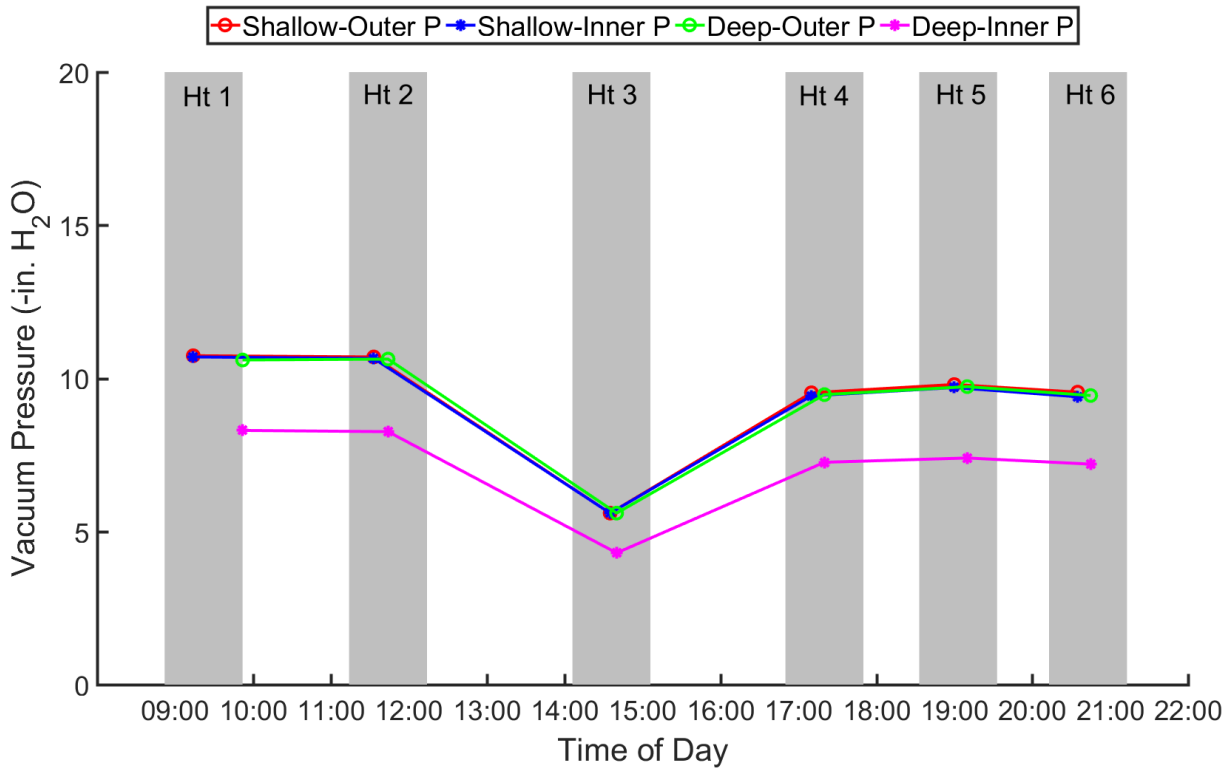

The measured fluxes were adjusted using the vacuum pressure data to analyze variation of flux solely with cover thickness without the effects of varying pressure during the tests. Adjustment factors were calculated for pressure using the relative ratio of the pressure for a given thickness to the maximum pressure obtained in the investigation. The measured flux increased with decreasing pressure from the maximum value. The adjusted fluxes are presented in Table 4.30, Figure 4.109, and Figure 4.110. The adjusted flux data demonstrated modest variations from the measured data with GHG fluxes varying more with cover thickness than NMVOC fluxes.

Table 4.34 – Variation in Cover Thickness Fluxes for Measured and Adjusted GHG and NMVOC Data

Cover Thickness (m)	Measured Mean GHG Flux (g/m^2-day)	ΔP Adjusted Mean GHG Flux (g/m^2-day)	Measured Mean NMVOC Flux (g/m^2-day)	ΔP Adjusted Mean NMVOC Flux (g/m^2-day)	Measured Median GHG Flux (g/m^2-day)	ΔP Adjusted Median GHG Flux (g/m^2-day)	Measured Median NMVOC Flux (g/m^2-day)	ΔP Adjusted Median NMVOC Flux (g/m^2-day)
0.37	$7.74x10^{0}$	$8.59x10^{0}$	$2.08x10^{-5}$	$2.31x10^{-5}$	$1.10x10^{-2}$	$1.23x10^{-2}$	$3.10x10^{-6}$	$3.44x10^{-6}$
0.70	$1.97x10^{0}$	$2.13x10^{0}$	$2.24x10^{-5}$	$2.43x10^{-5}$	$3.32x10^{-4}$	$3.60x10^{-4}$	$2.37x10^{-6}$	$2.57x10^{-6}$
1.00	$2.01x10^{0}$	$2.23x10^{0}$	$2.62x10^{-5}$	$2.91x10^{-5}$	$1.49x10^{-3}$	$1.65x10^{-3}$	$2.70x10^{-6}$	$3.00x10^{-6}$
1.29	$2.57x10^{0}$	$3.79x10^{0}$	$1.59x10^{-5}$	$2.34x10^{-5}$	$5.07x10^{-3}$	$7.48x10^{-3}$	$3.39x10^{-6}$	$5.01x10^{-6}$

Cover Thickness (m)	Measured Mean GHG Flux (g/m^2-day)	ΔP Adjusted Mean GHG Flux (g/m^2-day)	Measured Mean NMVOC Flux (g/m^2-day)	ΔP Adjusted Mean NMVOC Flux (g/m^2-day)	Measured Median GHG Flux (g/m^2-day)	ΔP Adjusted Median GHG Flux (g/m^2-day)	Measured Median NMVOC Flux (g/m^2-day)	ΔP Adjusted Median NMVOC Flux (g/m^2-day)
1.57	$3.39x10^{0}$	$3.39x10^{0}$	$3.58x10^{-5}$	$3.58x10^{-5}$	$1.07x10^{-3}$	$1.07x10^{-3}$	$6.17x10^{-6}$	$6.17x10^{-6}$
1.86	$3.42x10^{-1}$	$3.42x10^{-1}$	$1.22x10^{-5}$	$1.22x10^{-5}$	$-4.18x10^{-4}$	$-4.18x10^{-4}$	$1.19x10^{-6}$	$1.19x10^{-6}$

Figure 4.110 Adjusted Cover Thickness Data for a) GHG and b) NMVOC Fluxes at SMRL.

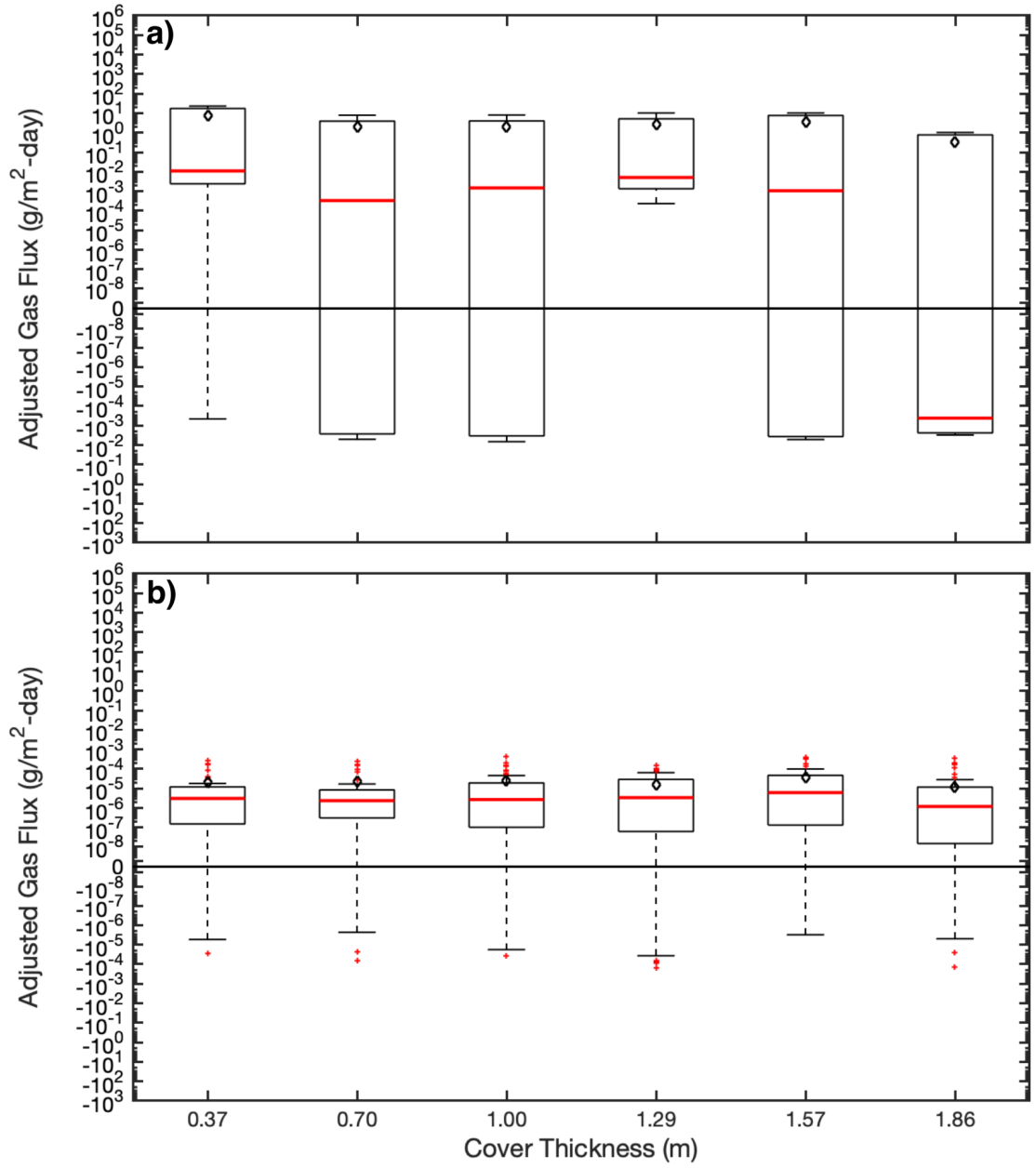

Figure 4.111 Measured and Adjusted Cover Thickness Flux Data for a) GHG and b) NMVOC Fluxes at SMRL.

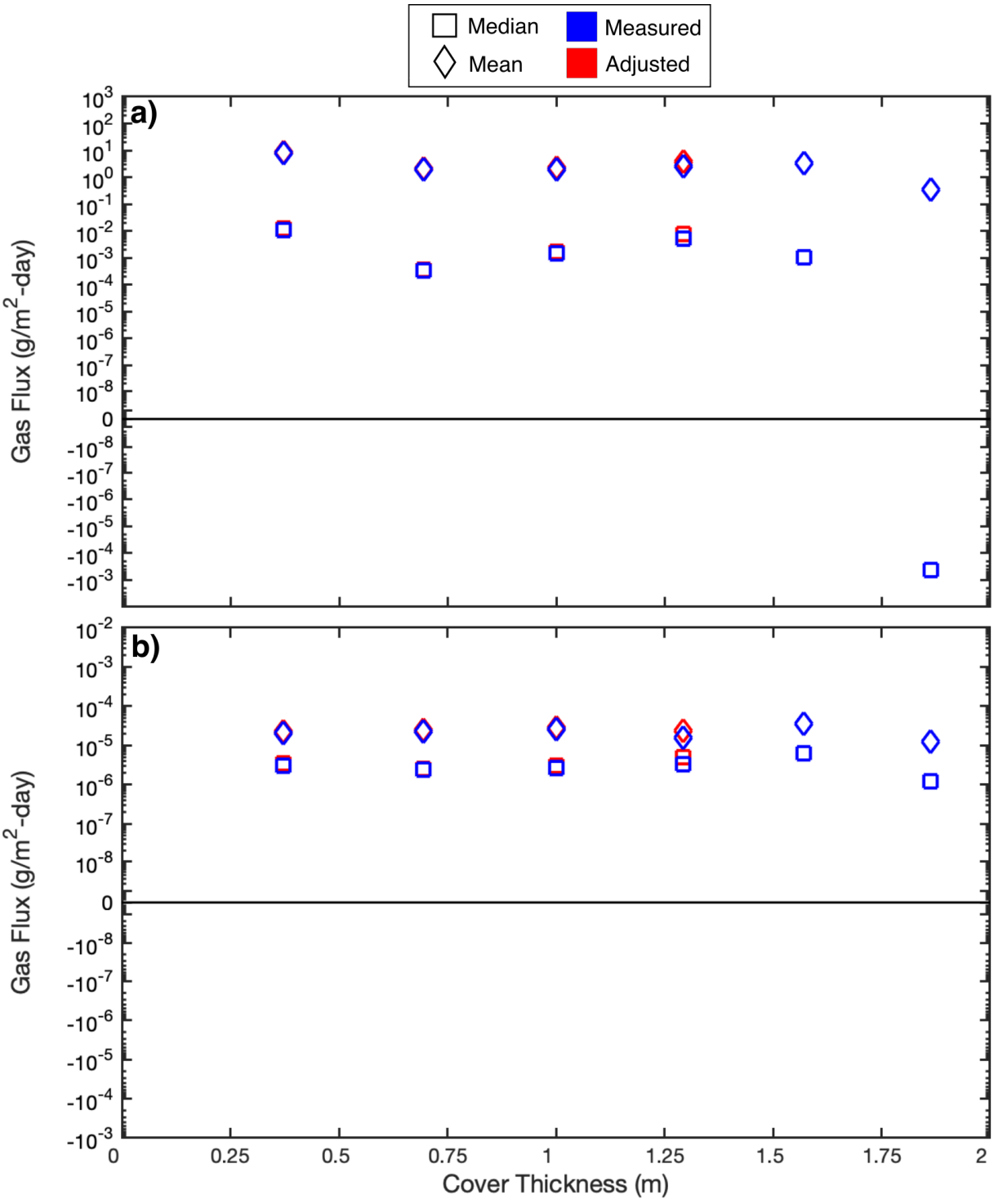

4.13.3 Temporal Surface Flux Variability Testing Results at SMRL

The GHG and NMVOC flux testing results for the temporal testing program are presented in Figure 4.111. For GHGs, based on median values, the daytime

measurements including the 1:15 PM measurement on October 21 and 1:30 PM measurement on October 25 were similar. The 6:30 PM measurement on October 25 also was in line with the midday measurements. The early morning measurement and the overnight measurement were higher than the daytime measurements. The mean fluxes at the different testing times were relatively similar over the five different measurement times. For NMVOCs, based on median values, the measurements were relatively similar except for the 1:30 PM measurement on October 25. The early morning and overnight measurement were somewhat higher than the daytime measurements. The mean NMVOC fluxes at the different testing times were relatively similar over the five different measurement times with slightly higher fluxes for the early morning and overnight measurements.

Figure 4.112 Results of the Temporal Flux Variability Testing for a) GHGs and b) NMVOCs at the SMRL during the Dry Season.

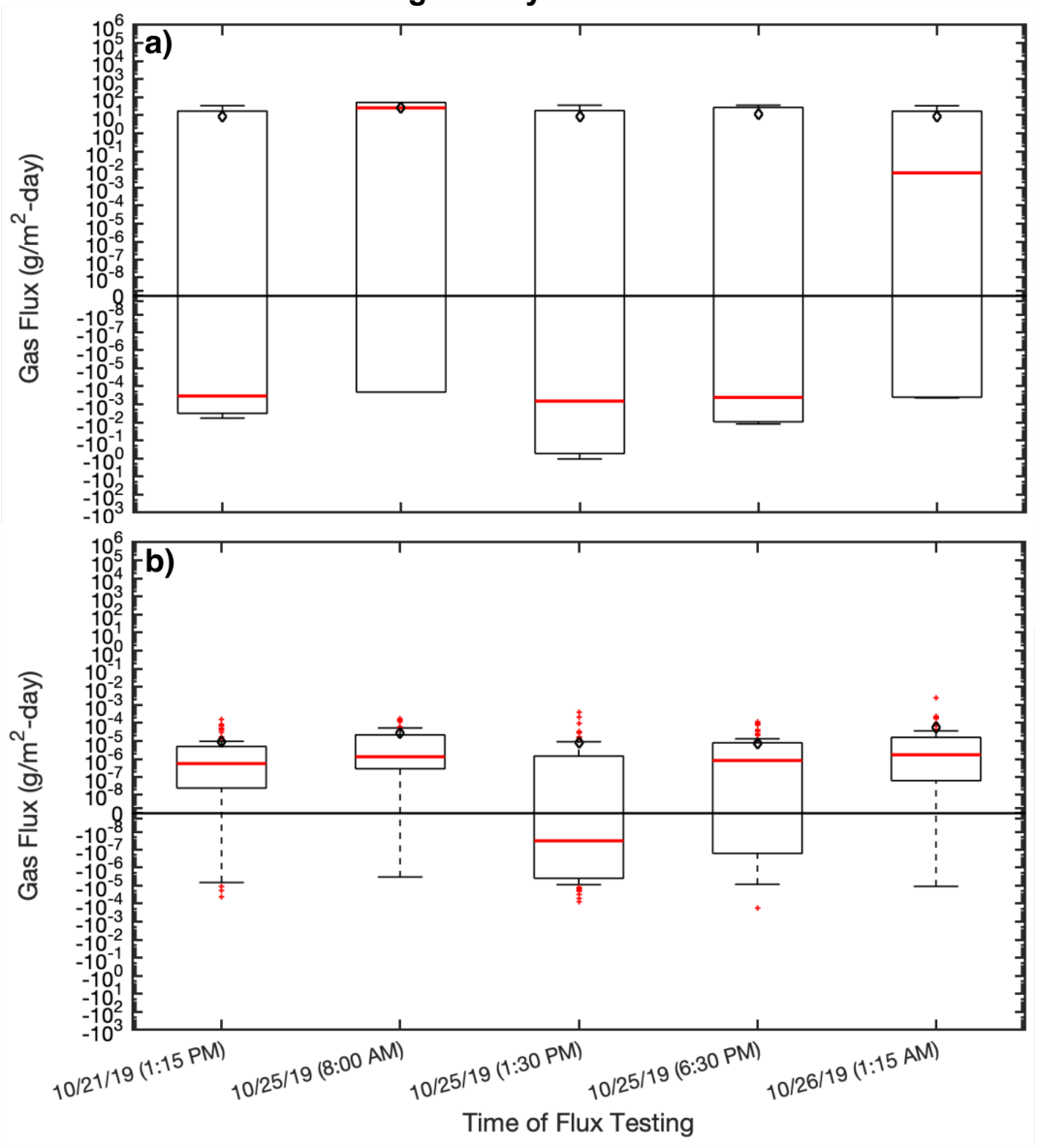

Diurnal variations in flux are assessed using 1:30 PM measurements on October 25 and 1:30 AM measurements on October 26. In line with the overall temporal flux variations described in the previous paragraph, fluxes of both NMVOCs and GHGs increased during the nighttime hours, where a larger difference was observed for the GHGs than the NMVOCs (Figure 4.111). For midday and overnight hours, the median flux for overall GHGs and NMVOCs were -6.73×10^{-4} to 6.44×10^{-3} as well as -3.26x10-8 to 1.73×10^{-6} g/m^2-day, respectively. For midday and overnight hours, the mean flux for overall GHGs and NMVOCs were 8.76×10^{0} to 8.44×10^{0} and 8.38×10^{-6} to 5.39×10^{-5} g/m^2-day, respectively. The variations in flux values likely resulted from a combination of variations in temperature, barometric pressure, and atmospheric chemistry. Optimum methane oxidation rates were associated with temperatures similar to the daytime temperatures (Figure 4.112) observed at the site, with significantly reduced oxidation rates at lower temperatures in line with nighttime temperatures at SMRL (Boeckx and van Cleemput 1996, Börjesson and Svensson 1997b). Barometric pressure was lower during nighttime (99.8 kPa) measurements than the daytime measurements (100.2 kPa) resulting in increased nighttime flux values. Atmospheric mixing is expected to be greater during the daytime, whereas nighttime is generally consistent with atmospheric stability (Yokouchi and Ambe 1988). Atmospheric hydroxylation (by OH radicals primarily) is more prominent in the daytime hours (when OH is produced from sunlight) (Mellouki et al. 2015). Increased transfer of gases from the ground surface to the troposphere and hydroxylation occurring during the daytime may have reduced ambient NMVOC concentrations near the surface of the landfill (depending on the reactivity of the NMVOC family among other factors).

The measured fluxes were adjusted using the vacuum pressure data (Table 4.31 and Figure 4.113) to analyze variation of flux solely with time without the effects of varying pressure during the tests. Adjustment factors were calculated for pressure using the relative ratio of the pressure at a given location to the maximum pressure obtained in the investigation. The measured flux increased with decreasing pressure. Measured and adjusted flux data for median and mean GHGs and NMVOCs are presented in Table 4.31. The trends observed for the measured and adjusted data were similar with somewhat more pronounced variations between flux values for the adjusted data (Table 4.31).

Table 4.35 – Variation in Temporal Fluxes for Measured and Adjusted Data GHG and NMVOC Data

Date and Time	Measured Mean GHG Flux (g/m^2-day)	ΔP Adjusted Mean GHG Flux (g/m^2-day)	Measured Mean NMVOC Flux (g/m^2-day)	ΔP Adjusted Mean NMVOC Flux (g/m^2-day)	Measured Median GHG Flux (g/m^2-day)	ΔP Adjusted Median GHG Flux (g/m^2-day)	Measured Median NMVOC Flux (g/m^2-day)	ΔP Adjusted Median NMVOC Flux (g/m^2-day)
10/21/19 1:13 PM	8.55×10^{0}	9.00×10^{0}	9.12×10^{-6}	9.59×10^{-6}	-3.50×10^{-4}	-3.68×10^{-4}	5.64×10^{-7}	5.93×10^{-7}
10/25/19 7:55 AM	2.58×10^{1}	2.68×10^{1}	2.74×10^{-5}	2.84×10^{-5}	2.58×10^{1}	2.68×10^{1}	1.33×10^{-6}	1.38×10^{-6}
10/25/19 1:34 PM	8.76×10^{0}	9.26×10^{0}	8.38×10^{-6}	8.85×10^{-6}	-6.73×10^{-4}	-7.11×10^{-4}	-3.26×10^{-8}	-3.44×10^{-8}

Date and Time	Measured Mean GHG Flux (g/m^2-day)	ΔP Adjusted Mean GHG Flux (g/m^2-day)	Measured Mean NMVOC Flux (g/m^2-day)	ΔP Adjusted Mean NMVOC Flux (g/m^2-day)	Measured Median GHG Flux (g/m^2-day)	ΔP Adjusted Median GHG Flux (g/m^2-day)	Measured Median NMVOC Flux (g/m^2-day)	ΔP Adjusted Median NMVOC Flux (g/m^2-day)
10/25/19 7:43 PM	$1.20x10^{1}$	$1.20x10^{1}$	$7.05x10^{-6}$	$7.05x10^{-6}$	$-4.20x10^{-4}$	$-4.20x10^{-4}$	$8.35x10^{-7}$	$8.35x10^{-7}$
10/26/19 2:16 AM	$8.44x10^{0}$	$8.65x10^{0}$	$5.39x10^{-5}$	$5.53x10^{-5}$	$6.44x10^{-3}$	$6.60x10^{-3}$	$1.73x10^{-6}$	$1.77x10^{-6}$

Figure 4.113 Variation in a) Vacuum Pressure at Shallow and Deep Waste Layers and b) Soil and Air Temperatures for the Temporal Testing Program at SMRL.

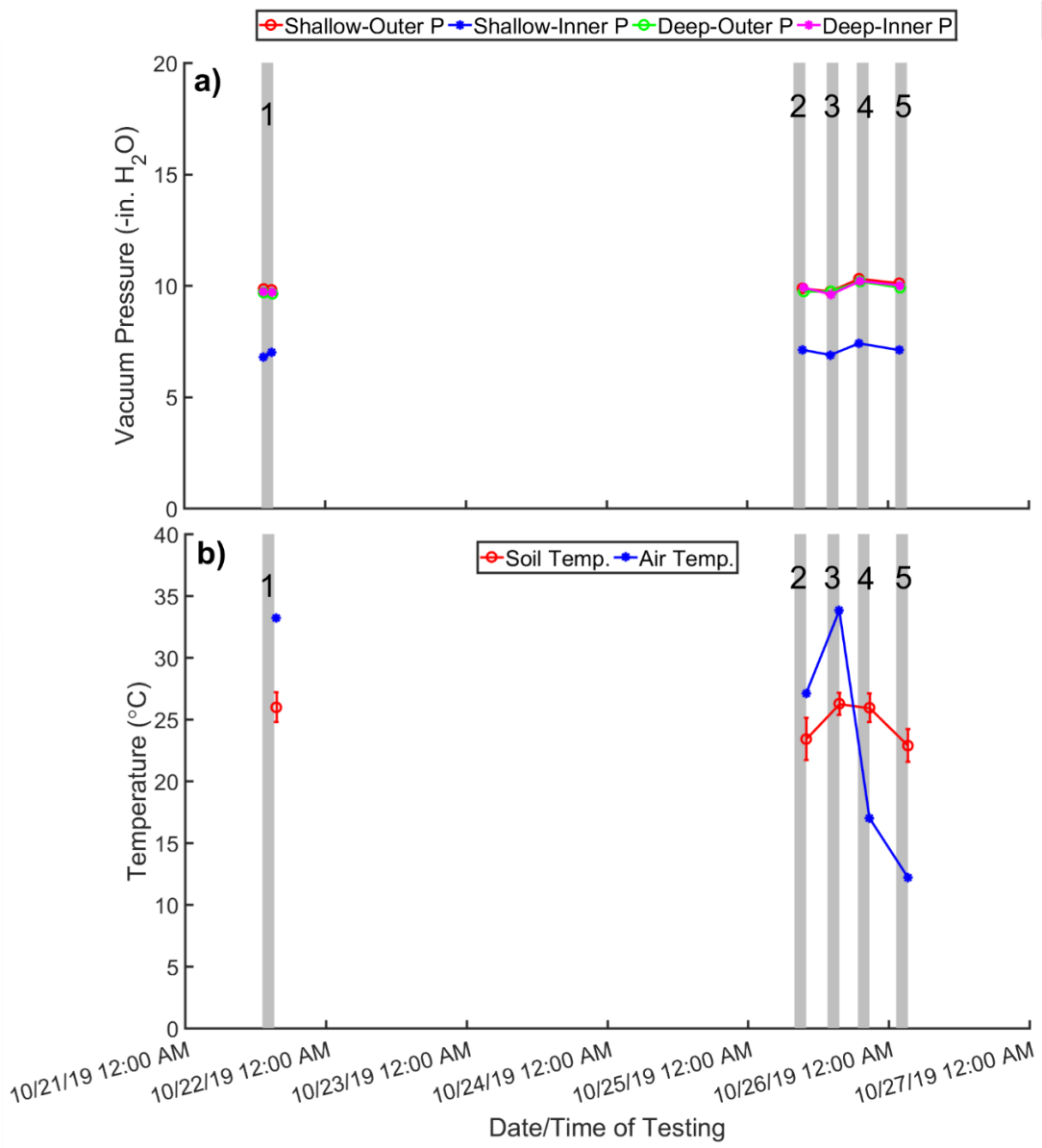

Figure 4.114 Measured and Adjusted Temporal Flux Data for a) GHG and b) NMVOC Fluxes at SMRL.

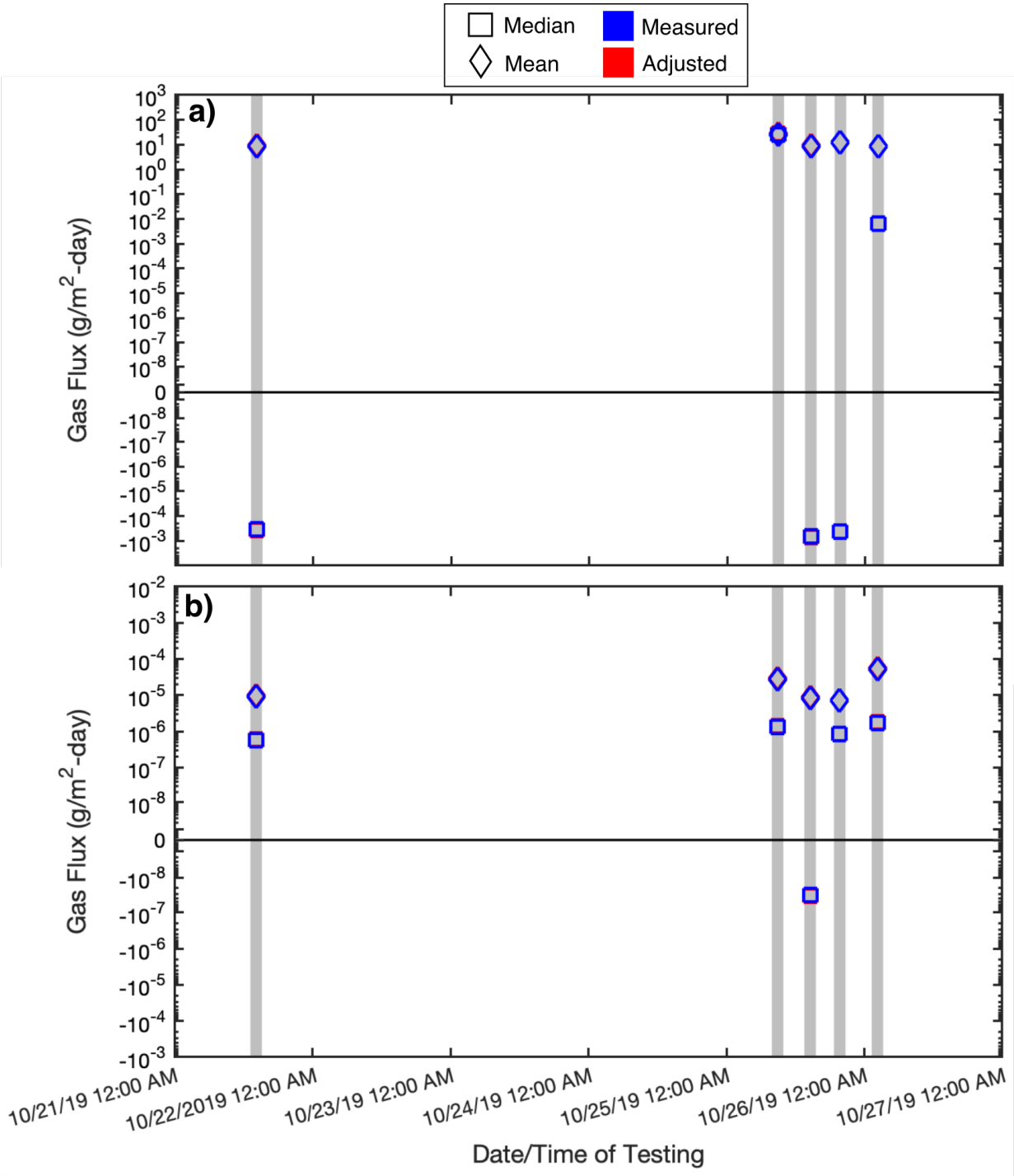

4.13.4 Contaminated, Non-Hazardous Soils Testing Results at SMRL

Figure 4.114 presents box plots by chemical family summarizing the flux measurements conducted across the extended daily and final cover testing locations at the NHIS portion of Santa Maria Regional Landfill during the dry season. Similar to

the MSW testing at SMRL as well as at the other four ground-testing sites, the highest fluxes were observed for GHGs. Following GHG fluxes, the alcohols, ketones, and aldehydes/alkynes had the highest fluxes (Figure 4.114). With the exception of the aldehydes/alkynes, the highly emitting NMVOC chemical families are not directly linked to volatile organic compounds derived from crude oil. The aromatics, alkanes, and alkenes likely were directly related to the petroleum hydrocarbons contained in crude oil. The variability in measured fluxes was generally higher for the aromatics and ketones, which demonstrated some probability of uptake over emissions as the IQR extended below zero.

Figure 4.115 Measured Fluxes at the NHIS Cells at Santa Maria Regional Landfill by Chemical Family in the Dry Season (open black diamonds, red lines, and solid red dots represent means, medians, and outliers, respectively).

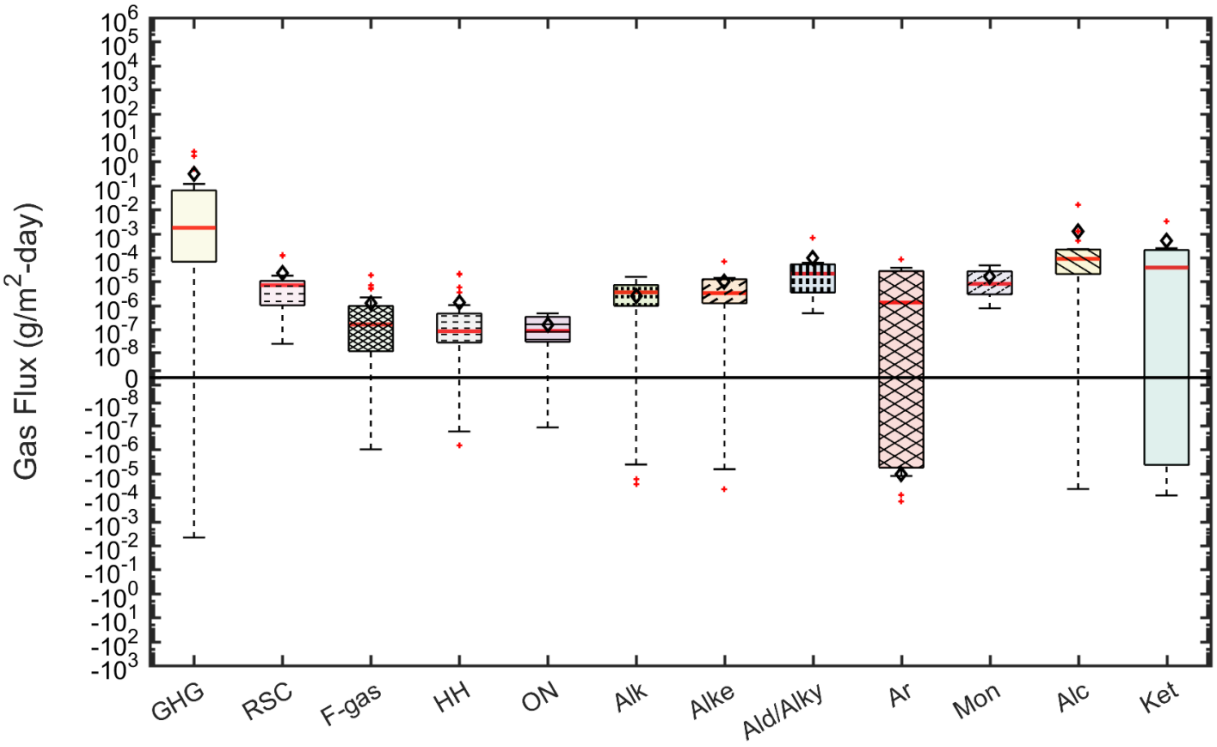

Fluxes by cover category from the NHIS cells are presented in Figure 4.115. Net uptake of methane was more probable over emissions for both of the cover categories tested. Methane and nitrous oxide fluxes were generally higher from the final cover than the extended daily cover. Based on median values presented in Figure 4.115, the NMVOC fluxes were generally higher from the final cover than the extended daily cover.

Figure 4.116 Measured Fluxes by Cover Category at the NHIS Cells at Santa Maria Regional Landfill in the Dry Season (open black diamonds, red lines, and solid red dots represent means, medians, and outliers, respectively).

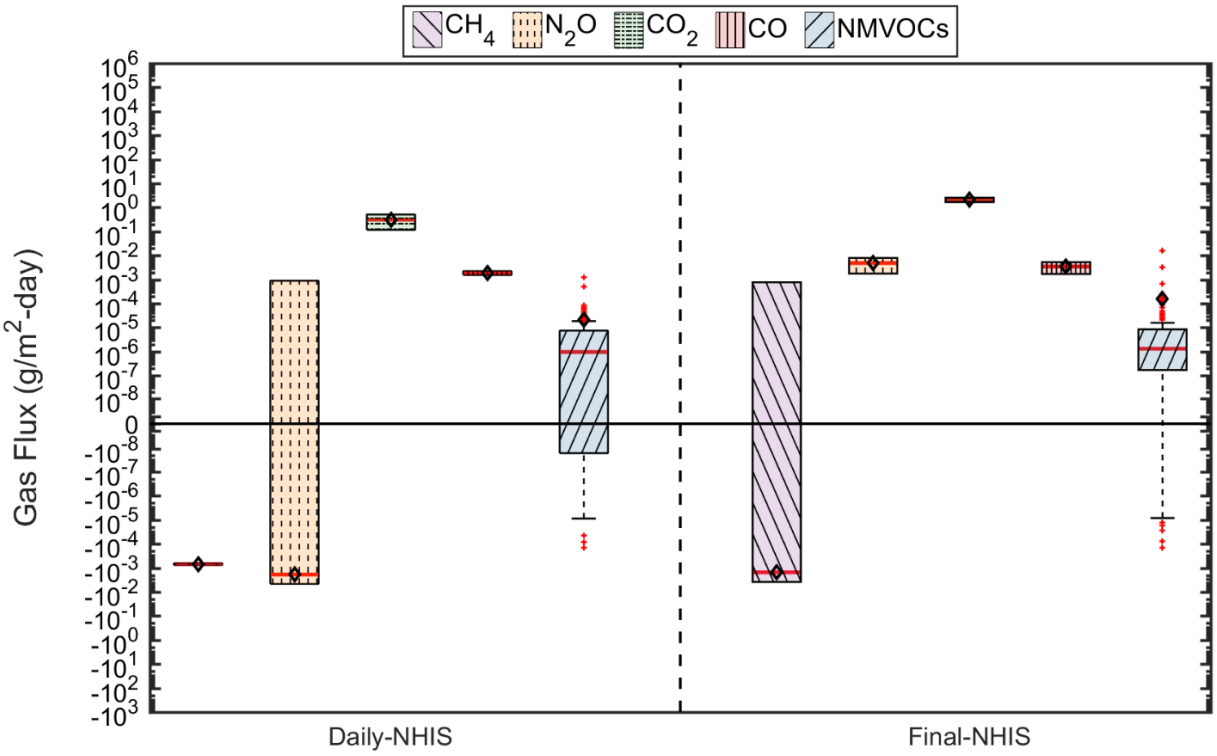

A comparison of daily and final cover flux data for the NHIS and the MSW cells are presented in Figure 4.116. For the daily covers, greenhouse gas fluxes were greatest from the cell receiving MSW. Fluxes of alkanes and alkenes were higher through the daily cover over the MSW compared to the daily cover over NHIS, whereas aldehydes/alkynes and aromatics fluxes were higher for the NHIS cell. For the final covers, GHG fluxes were higher from the NHIS cell than the MSW cell. Also, aromatic fluxes were significantly higher for NHIS than MSW with lower differences for the remaining NMVOCs.

Figure 4.117 Comparison of GHG, Alkane, Alkene, Aldehyde/Alkyne, and Aromatic Hydrocarbon Flux Measurements from a) Daily and b) Final Covers from the NHIS and MSW Cells at SMRL during the Dry Season.

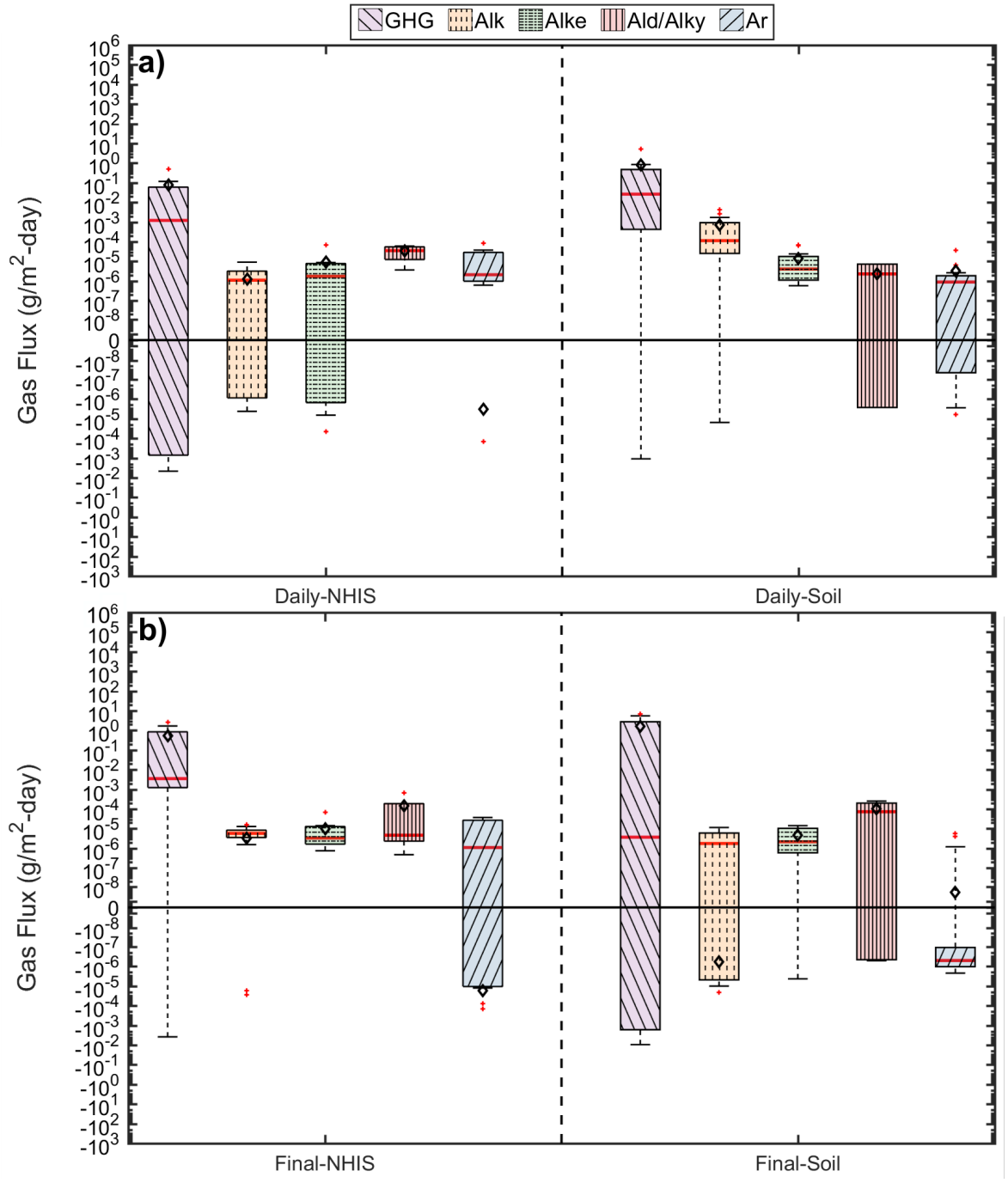

Based on results presented in Figures 4.114-4.116, high GHG fluxes are observed from the NHIS cells at SMRL in line with and even exceeding MSW cells. The high differences resulted from the flux of non-methane GHGs (e.g., nitrous oxide) as the methane fluxes from the NHIS cells were very low (Figure 4.115). Low methane flux is

expected at the NHIS cells as the emissions are mainly coming from the contaminated soils in these cells and not directly from MSW. Surface methane emissions are likely not occurring at the NHIS cells as the MSW at the bottom of these cells are old and also a bottom liner system was installed underneath the contaminated soils separating these from the underlying old MSW. The high GHG fluxes likely resulted from the biological processes naturally occurring in the cover soils at the NHIS cells. The flux of alkanes, alkenes, aldehydes/alkynes, and aromatics, expected to be present in the petroleum contaminated soils, were high from the NHIS cells. The highest differences for these NMVOCs between the NHIS and MSW were for aromatics (higher aromatics fluxes from the NHIS than MSW). The aromatics are the main species present in the petroleum contaminated soils and this is reflected directly in the measured fluxes at the site. The fluxes for alkanes, alkenes, and aldehydes/alkynes were relatively similar for the NHIS and MSW cells (Figure 4.116). Despite these similarities, the sources of these different chemical families, are different between the two areas of the landfill, where the fluxes from the NHIS cells are primarily anthropogenic (contaminated soil) in origin as compared to a mixture of anthropogenic and biogenic sources at the MSW cell. In addition to the four directly petroleum related NMVOCs, positive and high (e.g., alcohols and ketones) fluxes were obtained for the remaining seven NMVOCs investigated in the study (Figure 4.114). Various transformation processes including biological production in the soil cover may have contributed to the production of these chemicals. While the bottom liner system beneath the contaminated soils was likely effective against upward methane migration through the contaminated soils (also potentially the old MSW no longer produces significant methane), the different types of NMVOCs may have moved through the bottom liner materials (example of transport of VOCs through HDPE geomembranes provided above) contributing to the emissions of the NMVOCs from the NHIS cells.

4.13.5 Wet Waste Placement Testing Results at Teapot Dome Landfill

The results from additional tests conducted at the wet (i.e., winter) waste placement area at Teapot Dome Landfill in November 2019 are presented together with the August 2018 data from the same cell (Figure 4.117). Both data sets represent dry season tests at the site. The November 2019 fluxes were also high and in general similar to the data from the August 2018 tests with the exception of the low ketone measurements in November 2019.

Figure 4.118 Fluxes by Chemical Family from the Wet Waste Intermediate Cover at Teapot Dome Landfill in the Dry Season a) August 2018 Tests and b) November 2019 Tests (open black diamonds, red lines, and solid red dots represent means, medians, and outliers, respectively).

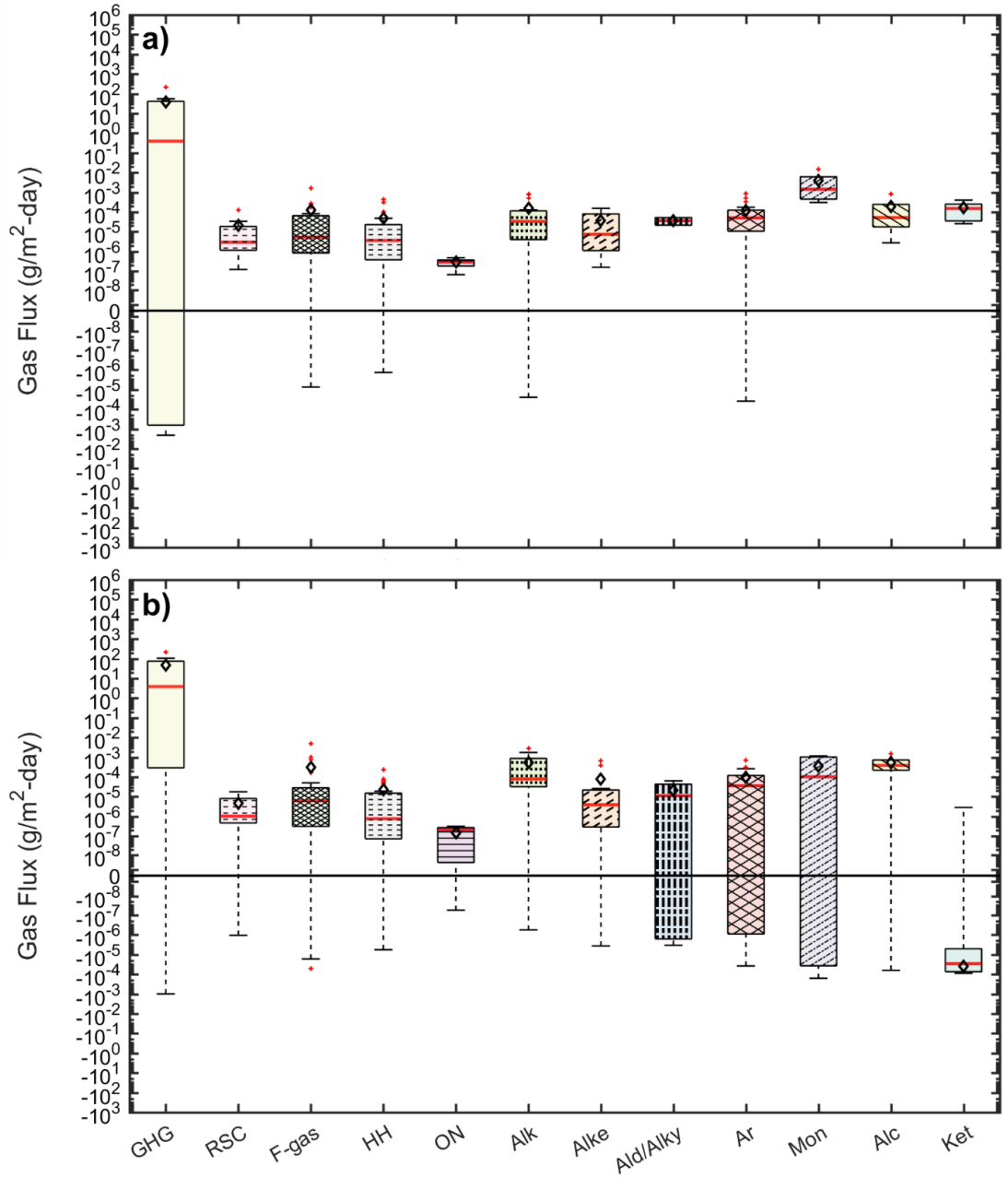

Individual GHG specie and overall NMVOC fluxes for the August 2018 and November 2019 tests are presented in Figure 4.118. The magnitude and variability of the individual GHGs and the overall NMVOCs were also high and in general similar to the August 2018 test results with the exception of the higher variation in nitrous oxide measurements in August 2018 compared to November 2019. Overall, the results presented in Figures 4.117 and 4.118 confirm that high emissions of GHG and

NMVOCs occur through the intermediate cover locations overlying wet waste placement areas at Teapot Dome landfill.

Figure 4.119 Individual GHG and Overall NMVOC Fluxes from the Wet Waste Intermediate Cover at Teapot Dome Landfill in the Dry Season a) August 2018 Tests and b) November 2019 Tests (open black diamonds, red lines, and solid red dots represent means, medians, and outliers, respectively).

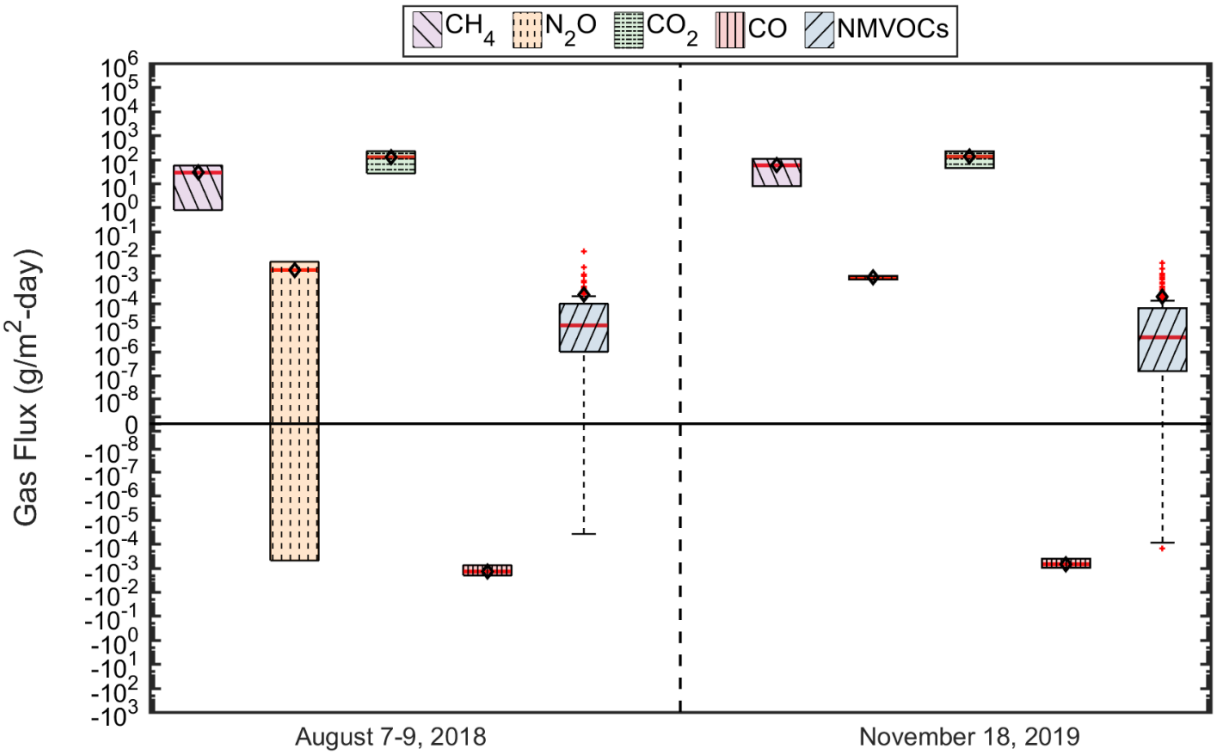

4.14 Comparison to California-Specific Modeling

An overview of methane generation, oxidation, and potential emissions from landfill cover soils in California is presented in Spokas et al. (2015). Spokas et al. (2015) identified a strong, linear relationship between average biogas recovery and WIP for 128 landfill sites in California (using 2010 WIP and reported landfill gas recovery estimates) with the slope of the regression line of 252.24×10^{-6} Nm^3 LFG $hr^{-1} Mg_{waste}^{-1}$. As observed in Figure 4.120, 4 out of the 10 sites from this study are predicted within the 95% confidence intervals of the empirical regression and the remaining 6 sites fall below the prediction zone. A linear regression was fit for the data in this study that resulted in a slope of 9.02×10^{-5} Nm^3 LFG hr^{-1} Mg_{waste}^{-1} (approximately a third of the value reported in Spokas et al. (2015)). While the trend for data from this study indicates positive correlation, the R^2 regression value for this trend was low at 0.36. The average CH_4 flux values from this investigation were 7.68, 4.8, and 0.0373 g/m^2-day for daily, intermediate, and final covers (which were two, one, and one orders of magnitude higher, respectively, than values reported by Spokas et al. (2015)).

Figure 4.120 Comparison of WIP vs. Biogas Recovery for all Landfills Investigated in this Study. The Blue and Red Lines Indicate the Replicated Mean and 95% CIs for the Linear Regression Presented in Spokas et al. (2015) for 128 Landfills in California. The Grey Values Indicate the Sites in this Study and the Green Line Indicates the Best Fitting Linear Regression.

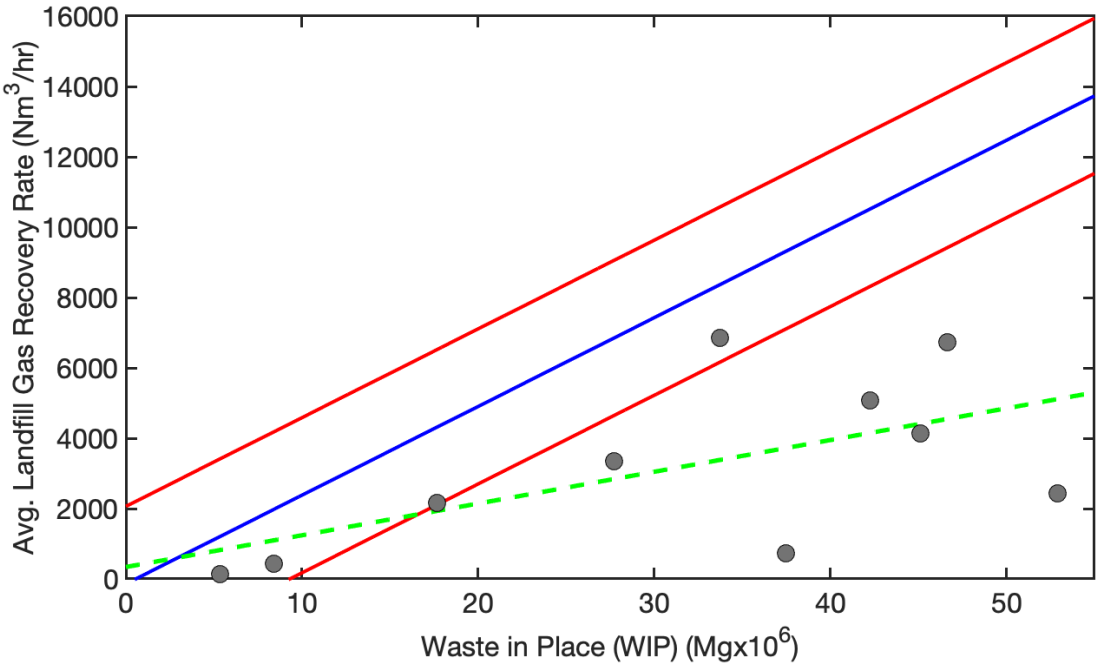

Spokas et al. (2015) further identified, through an intensive modeling effort of 381 landfill sites in California, that climatic variables such as precipitation and temperature were intimately related to methane flux. Regarding precipitation, the modeling results indicated that there was a strong non-linear relationship between methane flux and precipitation, where flux decreased as a function of precipitation. Spokas et al. (2015) also indicated that for sites receiving >500 mm of precipitation annually, the intermediate cover fluxes were all less than 15 g CH_4/m^2-day. As observed in a plot of measured fluxes with precipitation for this current investigation (Figure 4.121), a negative, non-linear correlation was observed for average intermediate cover fluxes, agreeing with results presented by Spokas et al. (2015). In addition, the only site in this study with annual precipitation greater than 500 mm was Potrero Hills landfill, where average methane flux from the intermediate cover was 2.15 g/m^2-day. Spokas et al. (2015) reported an approximately 17-fold difference between seasonal emissions based on monthly analysis. The seasonal variations from this investigation were within one order of magnitude and agreed well with the seasonal difference modeling presented by Spokas et al. (2015).

The differences between results from this study and results presented in Spokas et al. (2015) are attributed to the different approaches used in the studies: this investigation was field-measurement intensive for a limited number of sites and Spokas et al. (2015) was a modeling-intensive study with many sites and site-reported data.

Figure 4.121 Comparison of Annual Normal Precipitation (mm) and Average Flux from Intermediate Cover Locations at all 5 Ground-Based Landfill Sites.

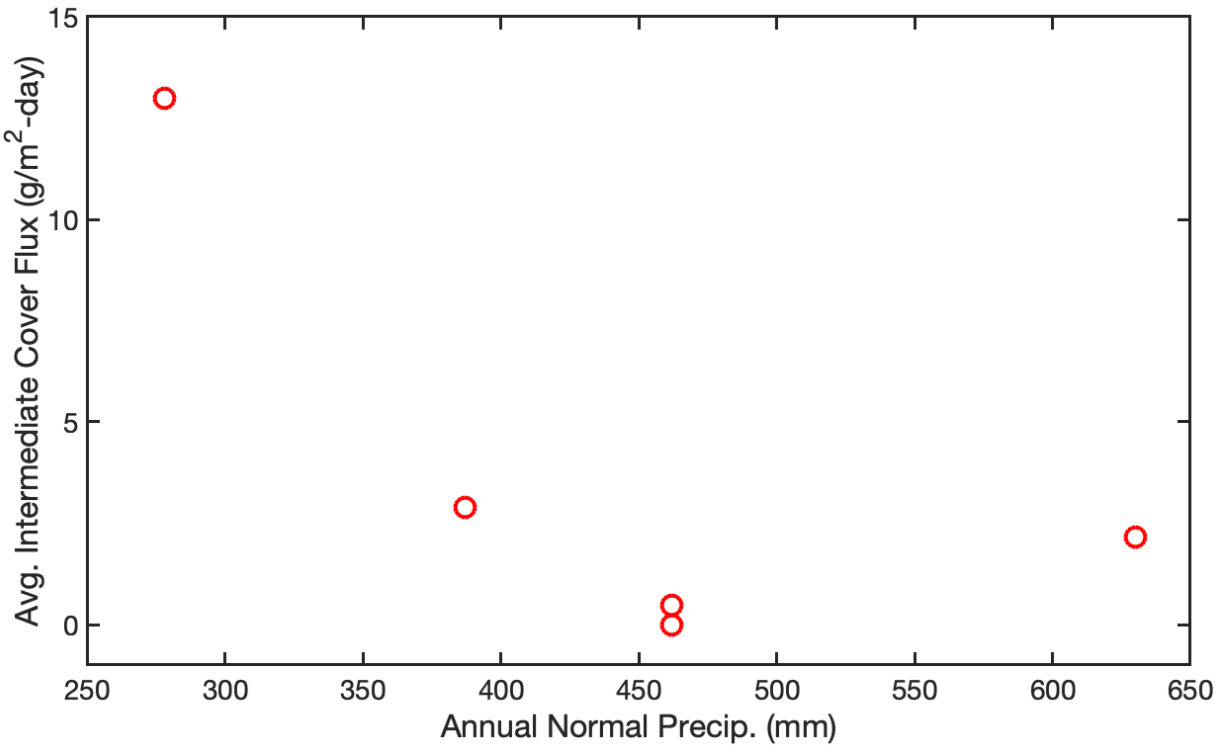

4.15 Presence of Vegetation

Vegetation was present in varying degrees on the covers at the locations selected for testing. A numerical rating scale has been developed to provide context in relation to the test results. Five categories of vegetative cover have been used:

- Woody vegetation (e.g., chipped green waste, construction and demolition waste): designated W;
- No vegetation (bare soil or other material such as auto fluff): designated 0;
- Live vegetation present: rated 1-10 based on areal coverage and growth of vegetation (1 corresponds to nearly bare, 10 corresponds to well vegetated and healthy growth);
- Dried vegetation present: rated 1-10, numerical value as described above for extent of vegetation, halved to reflect dried state of vegetation;
- Partially live, partially dried vegetation: rated using weighted average of numerical methods above.

Example photographs of tested covers with corresponding ratings are provided in Figure 4.122 below. A complete numerical summary of vegetation ratings for the entire test program is presented in Appendix C4.

Figure 4.122 Examples of Vegetation Ratings

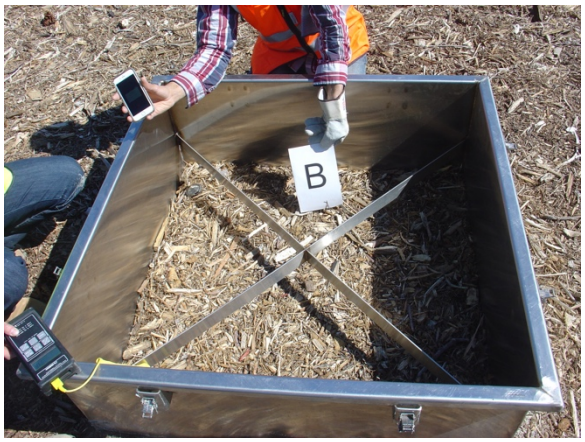

a) Vegetation Rating: W
[Woody Vegetation]

b) Vegetation Rating: W
[Woody Vegetation]

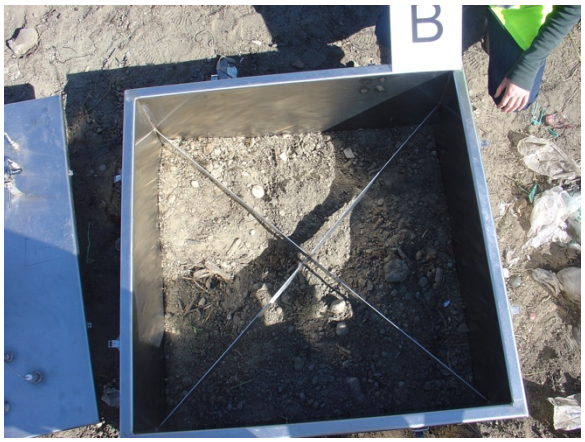

c) Vegetation Rating: 0/10
[No Vegetation]

d) Vegetation Rating: 0/10
[No Vegetation]

e) Vegetation Rating: 2/10
[Live Vegetation]

f) Vegetation Rating: 4/10
[Live Vegetation]

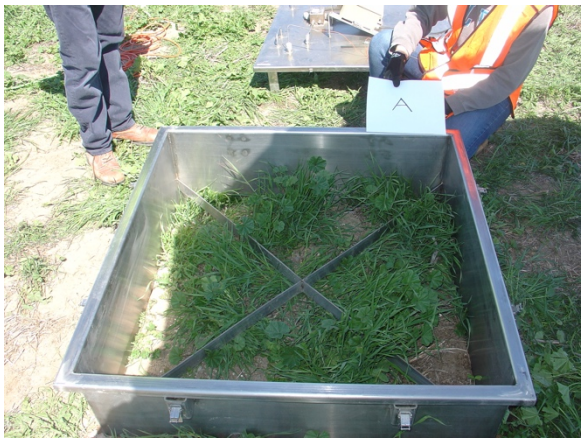

g) Vegetation Rating: 7/10
[Live Vegetation]

h) Vegetation Rating: 10/10
[Live Vegetation]

i) Vegetation Rating: 2/10
[Dried Vegetation]

j) Vegetation Rating: 4/10
[Dried Vegetation]

k) Vegetation Rating: 4.5/10
[Dried Vegetation]

l) Vegetation Rating: 5/10
[Dried Vegetation]

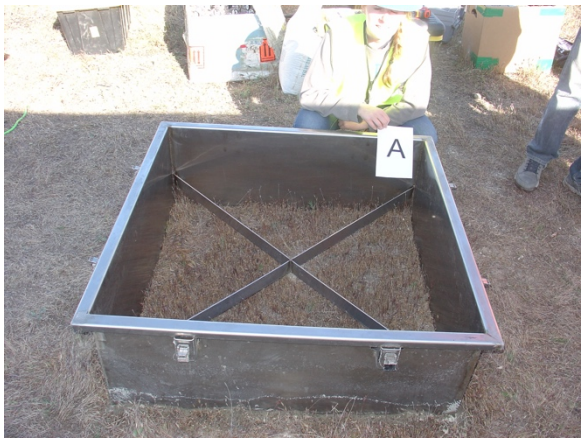

m) Vegetation Rating: 4/10
[Partially Live Vegetation]

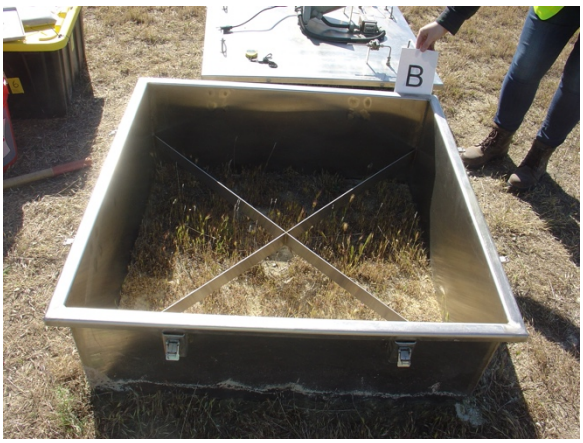

n) Vegetation Rating: 5/10
[Partially Live Vegetation]

Generally, soil and alternative daily covers were bare of vegetation. Interim covers had a mixture of bare condition and some vegetation. Final covers had vegetation present to varying degrees. The presence of vegetation has the potential to influence gas emissions from landfills through numerous mechanisms including disruption of soil structure in the root zone near the ground surface; uptake and production of chemicals through biological processes; uptake of CO_2 and production of O_2 due to photosynthesis; affecting near-surface ground temperatures due to shading, localized wind conditions, and evaporative cooling; modification of moisture conditions near surface due to moisture uptake/transpiration and shading from sun; and modification of air pressure conditions near the surface due to localized wind effects. These mechanisms contribute to differences in soil structure, air pressure conditions for advective flow, and chemical gradient conditions for diffusive flow.